

NPS ARCHIVE
1959
MUTO, C.

AN EXPERIMENTAL INVESTIGATION OF
THE EFFECTS OF HEAT TRANSFER
DURING CHARGING AND BLOWDOWN OF
SINGLE GAS RECEIVERS

CHARLES J. MUTO

AD 487800

AN EXPERIMENTAL INVESTIGATION OF
THE EFFECTS OF HEAT TRANSFER DURING
CHARGING AND BLOWDOWN OF SINGLE
GAS RECEIVERS

Charles J. Muto

AN EXPERIMENTAL INVESTIGATION OF
THE EFFECTS OF HEAT TRANSFER DURING
CHARGING AND BLOWDOWN OF SINGLE
GAS RECEIVERS

by

Charles J. Muto

//
Lieutenant, United States Navy

Submitted in partial fulfillment of
the requirements for the degree of

MASTER OF SCIENCE
IN
MECHANICAL ENGINEERING

United States Naval Postgraduate School
Monterey, California

1959

AN EXPERIMENTAL INVESTIGATION OF
THE EFFECTS OF HEAT TRANSFER DURING
CHARGING AND BLOWDOWN OF SINGLE
GAS RECEIVERS

by

Charles J. Muto

This work is accepted as fulfilling
the thesis requirements for the degree of

MASTER OF SCIENCE

IN

MECHANICAL ENGINEERING

from the

United States Naval Postgraduate School

ABSTRACT

Experimental data for both the charging and the blowdown process in a single air receiver is presented and interpreted in detail. The data indicate that heat transfer effects cause a radical departure from adiabatic behavior, and that such variances can be explained qualitatively on the basis of available simplified expressions for the state of a gas in a receiver. It is shown that the behavior of systems fulfilling the limiting conditions of these solutions can be adequately predicted and useful design results obtained. Methods for determining heat transfer convective conductances for use in the simplified solutions are discussed and evaluated.

The experimental work was performed from January 1959 through April 1959 at the United States Naval Postgraduate School, Monterey, California

ACKNOWLEDGEMENT

The author wishes to express gratitude to Professor C. P. Howard for his assistance and advice throughout the investigation both in the assembly of the test equipment and in the interpretation of the results. Indebtedness is also due Messrs. R. P. Kennicott and J. Beck for their work in the construction and installation of the experimental equipment.

TABLE OF CONTENTS

Item	Title	Page
Chapter 1	Introduction	1
Chapter 2	Objectives	3
Chapter 3	Description of Test Equipment	4
Chapter 4	Experimental Procedure	7
Chapter 5	Theoretical Considerations	9
Chapter 6	Summary of Experimental Results	15
Chapter 7	Discussion of Results	18
Chapter 8	Conclusions	38
Chapter 9	Recommendations	40
	Bibliography	41
Appendix I	Derivation of Solutions	42
Appendix II	Figures 1-14	49
Appendix III	Solution of General Blowdown Equation by Analog Computer	64
Appendix IV	Experimental Data	68

LIST OF ILLUSTRATIONS

FIGURE	TITLE	PAGE
1	Arrangement of Test Apparatus	50
2	Diagram of the Insulated Tank	51
3	Photograph of Test Apparatus	52
4	SR-4 Strain Gage Pressure Pickup	53
5	Test Results for Charging Uninsulated Tank, T^* vs. M^*	54
6	Test Results for Blowdown Uninsulated Tank, T^* vs. M^* , Runs 5 and 6	55
7	Test Results for Blowdown Uninsulated Tank, T^* vs. M^* , Runs 7 and 8	56
8	Test Results for Charging Insulated Tank, T^* vs. M^*	57
9	Test Results for Blowdown Insulated Tank, T^* vs. M^*	58
10	Test Results for Charging Insulated Tank with Added Capacitors, T^* vs. M^*	59
11	Test Results for Blowdown Insulated Tank with Added Capacitors, T^* vs. M^*	60
12	Predicted Average Convective Conductances During Charging Uninsulated Tank	61
13	Predicted Average Convective Conductances During Blowdown Uninsulated Tank	62
14	Effect of Tank Liner on C_0^* During Charging Run 17	63
15	Analog Computer Setup for Solution of General Eqn. for Constant Flow Blowdown	66

LIST OF TABLES

TABLE	TITLE	PAGE
1	Physical Dimensions of Experimental Apparatus	6
2	Summary of Uninsulated Tank Runs	15
3	Summary of Insulated Tank Runs	16
4	Summary of Insulated Tank Runs with Added Capacitors	17
5	Charging Conductances- Uninsulated Tank	19
6	Blowdown Conductances- Uninsulated Tank	25
7	Charging Conductances- Insulated Tank	28
8	Blowdown Conductances- Insulated Tank	30
9	Charging Conductances- Added Capacitors in Insulated Tank	32
10	Blowdown Conductances- Added Capacitors in Insulated Tank	35
11	Charging Run Data- Uninsulated Tank	69
12	Blowdown Run Data- Uninsulated Tank	71
13	Charging Run Data- Insulated Tank	73
14	Blowdown Run Data- Insulated Tank	74
15	Charging Run Data- Insulated Tank with Added Capacitors	76
16	Blowdown Run Data- Insulated Tank with Added Capacitors	78

SYMBOLS AND UNITS

English Letter Symbols

a	Scale factor
A	Area, ft^2
b	Width dimension, in.
C	Constant
C_c	Thermal capacitance of receiver shell, $\text{Btu}/^\circ\text{R}$
c_p	Specific heat at constant pressure, $\text{Btu}/(\text{lb}^\circ\text{R})$
c_v	Specific heat at constant volume, $\text{Btu}/(\text{lb}^\circ\text{R})$
d	Orifice diameter, in.
D	Diameter of receiver, in.
G	Mass velocity, $\text{lb}/(\text{hr ft}^2)$
h	Specific enthalpy, Btu/lb
h	Unit heat transfer convective conductance, $\text{Btu}/(\text{hr ft}^2{}^\circ\text{R})$
I	Jet momentum, defined in equation (18)
k	Thermal conductivity, $\text{Btu}/(\text{hr ft}^2{}^\circ\text{R}/\text{ft})$
K	Constant
L	Length dimension, ft.
M	Mass, lb.
P	Pressure, lb/ft^2
Q_s	Heat stored in insulation, Btu
q	Heat transfer rate, Btu/hr
R	Total heat transfer resistance, $\text{hr }^\circ\text{R}/\text{Btu}$
(R/m)	Universal gas constant/molecular mass of gas, $\text{ft lb}/(\text{lb}^\circ\text{R})$
t	Time
T	Absolute temperature, $^\circ\text{R}$
U	Total internal energy, Btu

English Letter Symbols

u	Specific internal energy, Btu/lb
\bar{u}	Average velocity, ft/sec.
V	Volume, ft ³
w	Mass flow rate, lb/hr
x, r	Cylindrical coordinates

Greek Letter Symbols

α	Constant
β	Temperature expansion factor, 1/°R
γ	Constant
δ	Constant
θ	Constant
μ	Viscosity, lb/hr ft)
ρ	Density, lb/ft ³
Δ	Denotes a difference

Nondimensional Grouping

$$C_o^* = C_c / (M_o c_v)$$

$$K k = c_p / c_v$$

$$M^* = M / M_o$$

$$NTU = 1 / (R_i c_v w_o) = (hA)_i / c_v w_o$$

$$NTU_\infty = 1 / (R_\infty c_v w_o) = (hA)_\infty / c_v w_o$$

$$P^* = P / P_o$$

$$T^* = T / T_o$$

$$T_i^* = T_i / T_o$$

$$T_c^* = T_c / T_o$$

$$T_\infty^* = T_\infty / T_o$$

$$w^* = w / w_o$$

$$Gr = \text{Grashof Number} \quad (L^3 \rho^2 g \beta \Delta T / \mu^2)$$

Nondimensional Grouping

Pr = Prandtl Number ($\mu c_p / k$)

Re = Reynolds Number ($D_x G / \mu$)

Subscripts

- o Refers to initial conditions
- l Refers to inlet state
- c Refers to capacitance
- i Refers to conditions inside receiver
- ∞ Refers to environmental conditions outside receiver
- x Refers to conditions at a distance x
- o,o Refers to conditions at the origin of a jet
- x,o Refers to conditions at a point on a jet axis
- x, r Refers to conditions at a point in an annulus
- m Refers to a mean value over a time period
- ave Refers to an average value at a given time

1. Introduction

During blowdown and charging of a gas receiver, changes in the gas temperature may provide a substantial temperature difference for heat transfer between the gas and the receiver walls. In addition to heat transfer through the walls, the receiver mass itself may provide significant energy storage so that heat transfer from such a thermal mass becomes important. Since the thermal capacitance of the receiver is usually quite large relative to that of the contained gas, considerable heat transfer between the walls and the gas can occur with little change in the wall temperature. The usual approach in the design of charging and blowdown systems has been to assume an adiabatic process. Inasmuch as this procedure neglects heat transfer effects, substantial error in the prediction of system behavior may result.

When heat transfer rates are to be considered, it becomes necessary to specify the rate at which mass enters or leaves the receiver. Two types of flow of considerable interest are constant mass flow and flow through a critical flow nozzle. The former case finds considerable application in the blowdown wind tunnel. Here the problem consists of maintaining sufficiently constant stagnation conditions despite decreasing temperature from the expansion process in the reservoir. Methods applicable to this problem have been treated both analytically and experimentally by Murphy, et al., [1]¹ employing a separate thermal mass and air storage reservoir. Incorporated in these solutions are analytical expressions for specific modes of convection heat transfer between the air, reservoir walls, and thermal mass. Thus the value of these solutions is limited to systems behaving in a similar manner.

¹Numbers in brackets refer to references listed in the bibliography.

Of perhaps more general interest are the solutions presented by Reynolds [2] for both constant and critical mass flows. These solutions employ a number of simplifying assumptions, the value of which are primarily dependent upon the accuracy of independently determining the heat transfer conductances between the gas, thermal mass, and environs. The assumption is made that the heat transfer resistances are uniform over all interior and exterior heat transfer surfaces and either invariant or independently predictable with time depending upon application. Critical flow blowdown experiments have been performed using time average free convection relationships which closely approximate the conductances predicted from these solutions [3].

Little other published information is available for similar charging and blowdown experiments. In receivers densely packed with heat capacitors, forced convection heat transfer correlations may apply. The fluid jet during charging may strongly influence the convection heat transfer mechanism. Imperfect mixing may occur during charging and cause temperature gradients within the system.

2. Objectives

Controlled single gas receiver charging and blowdown experiments were conducted at various mass flow rates and over varying ranges of thermal capacitance in order to accomplish the following objectives:

(a) Evaluate previously developed simplified analytical expressions for the thermodynamic state of the gas as a function of time.

(b) Determine the mechanism of heat transfer between the gas in the receiver and the receiver walls during these processes.

(c) Investigate analytical methods of predicting heat transfer conductances for use with the expressions for the thermodynamic state of the gas.

(d) Determine the feasibility of attaining an adiabatic process within a reasonable charging or blowdown time.

(e) Investigate the temperature distribution in the receiver as affected by mixing during charging.

3. Description of Test Apparatus

3.1. General Description

The test apparatus consisted of two 180 gallon pressure vessels of 150 psig test, one of which contained an internal liner of 5/8 in. California redwood. The tanks were arranged as shown in Fig. 1 with charging air introduced at the bottom through various size orifice plates. Each tank was fitted at the top with alternative piping arrangements for either critical or constant mass flow blowdown as shown in Fig. 2. Physical dimensions are contained in Table 1, page 6 . Air for charging the tanks was supplied from an air bank through a pressure regulator set at 200 psig. Metal strips could be inserted vertically in the tanks to serve as thermal capacitors. Pressure and temperature were continuously recorded with time. A photographic view of the general system is contained in Fig. 3.

3.2. Flow Metering

Sharp edge orifice plates were available in increasing diameters ranging from 1/8 in. through 1/2 in. for interchangeable mounting in flanges attached to the tank top and bottom. Discharge coefficients for orifice sizes through 1/4 in. diameter were determined over a range of pressure ratios using a separate blowdown calibration system. These coefficients remained fairly constant up to the critical pressure ratio. Discharge coefficients for the larger orifices were not determined because of limitations in the calibration system. Instead, experimental data from actual charging and blowdown runs was used to determine average flow rates during constant flow. Constant flow charging runs up to 100 psig tank pressure were attainable from an air bank supply of 200 psig pressure, at close to ambient temperature, upstream from the orifice. Separate

arrangements permitted either critical or constant mass flow blowdown. The tank top could be fitted with a flange arrangement containing a seated orifice plate and a 1 in. quick opening gate valve for critical flow runs. Also available for constant mass flow blowdown was a 1 in. copper pipe and flange arrangement equipped with a hand valve and bourdon pressure gage upstream from the orifice plate for maintaining the desired pressure ratio.

3.3. Temperature Measurements

Each tank was equipped with six 30 gage copper-constantan thermocouples. Four of these were arranged in series and spaced at equal volumes vertically in the tank to give an average tank air temperature. The two remaining junctions were available for monitoring wall or thermal capacitor temperature. Separate thermocouples were available for monitoring both constant flow charging and constant flow blowdown air stagnation temperature upstream from the orifice plates. Tank air and capacitor temperatures were recorded either on a continuously indicating Brown or on a Leeds Northrup potentiometer.

3.4. Pressure Measurements

Pressure was recorded from the output of a strain gage pressure pickup of the diaphragm type [4]. This pickup consisted of a seated diaphragm containing a center mounted SR4-A X 5 strain gage, together with two peripheral SR4-A5 gages as shown in Fig. 4. This arrangement was wired to form a four gage external bridge and provided a double output with temperature compensation. Calibrated sensitivity was 30 micro-inches per in. per psi. Output from the pickup was recorded on a Baldwin strain recorder. A bourdon gage was mounted directly on the tank for quick visual inspection of pressure.

TABLE I

Physical Dimensions of Experimental Apparatus

1. Uninsulated Tank

Volume: 23.9 ft³
 Internal area: 45.5 ft²
 Nominal internal diameter: 31 in.
 Nominal internal height: 54 in.
 Thermal mass: 835 lbs

2. Insulated Tank

Volume: 17.0 ft³
 Internal area: 38.0 ft²
 Nominal internal diameter: 29.5 in.
 Nominal internal height: 42 in.

3. Redwood Insulation

Thickness: 5/8 in.
 Density: 25 lbs/ft³
 Thermal Conductivity: 0.06 Btu/(hr ft °R)
 Specific heat: 0.6 Btu/(lb °R)
 Diffusivity: 0.004 ft²/hr

4. Strip Capacitors

Material: 24 S Aluminum (Alclad)
 Mass: 10.0 lbs
 Area: 108 ft²
 Gage: 0.012 in.

4. Test Procedure

Experimental work consisted of the following charging and blow-down runs:

a. Charging and blowdown of the insulated tank under close to adiabatic conditions (no internal heat capacitors), but with some heat transfer to and from the redwood insulation.

b. Charging and blowdown of the insulated tank with added heat capacitors and at constant mass flow rates to provide a finite capacitance with negligible inside heat transfer resistance.

c. Charging and blowdown of the uninsulated tank at constant flow rates such that the tank walls provided an isothermal sink and source with a finite inside heat transfer resistance.

In making a series of runs, the air bank was first charged with 290 psig air from a reciprocating air compressor and allowed to cool to ambient temperature. The air bank was then drained of any condensed water, and the pressure regulator set at 200 psig. A quick opening valve between the tank orifice and pressure regulator was then opened for a constant mass flow charge through the selected orifice plate. The piping system between the air bank and tank was of sufficient thermal capacitance that the air entered at nearly ambient temperature despite the blowdown process of the air bank. After reaching the desired tank pressure of about 100 psig, the tank was immediately blown down through either the critical flow quick opening valve or the constant flow hand valve arrangement. The latter process consisted of continually controlling the hand valve upstream of the blowdown orifice plate such that the upstream pressure remained constant at 30 psig. Once again, the piping and valve arrangement was of sufficient thermal capacitance that the temperature upstream from the orifice remained nearly ambient.

Throughout a typical cycle of charge and blowdown, tank air temperature was recorded at 5 sec. intervals with the Brown recorder and tank air pressure recorded continuously with the Baldwin recorder. Runs with added capacitors were repeated under identical conditions, recording the temperature of the capacitors with the Brown recorder. Runs varied in length from 11 to 240 seconds. Smooth curves were drawn through the recorded data plots. The flow rate was computed either from the usual critical flow metering equation using previously determined discharge coefficients or from the experimental mass-time data.

5. Theoretical Considerations

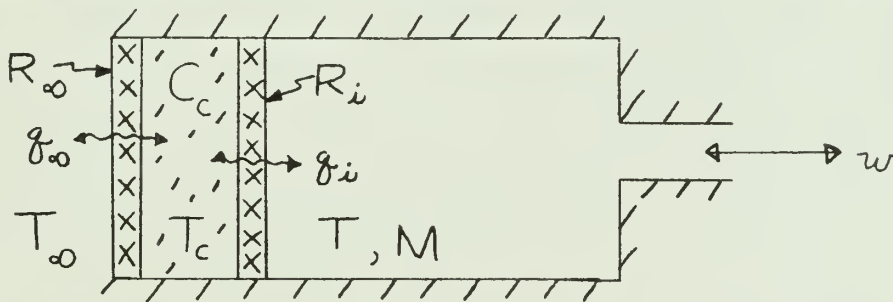
5.1. General

The objective of analyses of blowdown and charging systems is to obtain relations expressing the thermodynamic state of the gas in the receiver as a function of time. It is usual to use temperature as the dependent variable with mass content as the independent variable. For a constant volume receiver, the pressure, temperature, and mass content are related by the perfect gas equation of state:

$$PV = M(R/m)T \quad (1)$$

Thus having found temperature as a function of mass the pressure may also be found as a function of mass, and knowing the mass-time relationship, all state functions may be expressed as functions of time. We shall be concerned in this investigation primarily with constant mass flow.

General charging and blowdown solutions have been presented by Reynolds [2] using the following model:



These analyses assume that the state of the gas is uniform throughout the receiver and that the thermal capacitance of the receiver walls and other internal contents can be lumped into a single capacitance, $C_c = M_c c_p$. The heat transfer resistance between the capacitance and the environment is denoted by R_∞ and the resistance between the capacitance and the air in the tank by R_1 . The mass of gas in the tank is M and the mass flow rate is w .

Assuming that R_∞ , R_i , and C_c are invariant in time, a combination of energy balance and heat transfer rate equations leads to the general equation¹ for charging and blowdown at constant mass flow of the form:

$$M^* \frac{d^2 T^*}{dM^{*2}} + \alpha \frac{dT^*}{dM^*} + \gamma M^* \frac{dT^*}{dM^*} + \delta T^* + \theta = 0 \quad (2)$$

The constants α , γ , δ , and θ are functions of the system parameters NTU , NTU_∞ , and C_o^* . These parameters are defined as follows:

$$NTU = \frac{1}{R_i c_v w_o} = \frac{(hA)_i}{w_o c_v} \quad (3)$$

$$NTU_\infty = \frac{1}{R_\infty c_v w_o} = \frac{(hA)_\infty}{w_o c_v} \quad (4)$$

$$C_o^* = \frac{M_c c_p}{M_o c_v} = \frac{C_c}{M_o c_v} \quad (5)$$

The NTU groupings are the familiar "number of transfer units" used in heat exchanger analysis and represent dimensionless conductances (reciprocal of resistance) and also serve as a measure of the rate of heat transfer of the process. The C_o^* parameter represents the ratio of the capacitance of the receiver walls and internal thermal mass to the initial capacitance of the gas.

While equation (2) may be solved by analytical, graphical, and analog computer² methods, the use of such solutions for engineering applications is often difficult or impracticable. In the majority of engineering applications the magnitude of the system parameters NTU , NTU_∞ , and C_o^* may be such that more useful closed form solutions may be obtained.

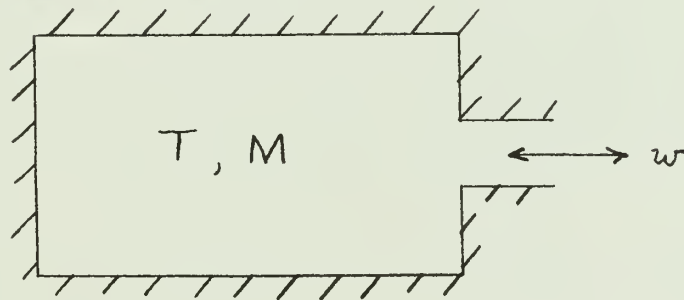
¹ See Appendix I for the derivation of the general equation.

² An analog computer method for the solution of the general equation for blowdown is presented and evaluated in Appendix III.

Several of these solutions have been developed by Reynolds [2] from basic principles, and it is with the application and evaluation of these solutions for constant flow that this thesis is concerned. Only the resultant expressions for temperature as a function of mass content will be given in this section for the application of interest. For convenience, the derivations of the general and of the simplified solutions are contained in Appendix I.

5.2. Adiabatic Charging and Blowdown

If there is no heat transfer to or from the gas, the process within the tank is adiabatic. An adiabatic process might be approximated during a very rapid charge or discharge, or during a relatively slow process with a receiver lined with an insulator between the gas and wall capacitance. Adiabatic behavior corresponds to the situation where $C_o^* = 0$ and $NTU_\infty = 0$, or when $NTU = 0$. Since no heat transfer is involved, the system is independent of mass flow rate. The following simple model and solutions apply:



charging

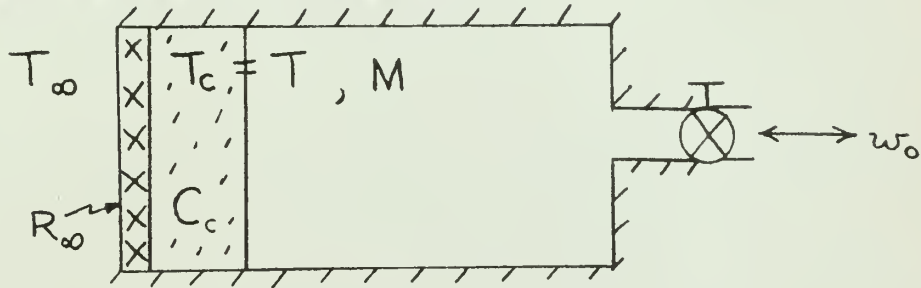
$$T^* = k T_i^* - \frac{k T_i^* - 1}{M^*} \quad (6)$$

blowdown

$$T^* = M^{*(k-1)} \quad (7)$$

5.3. Charging and Blowdown with Negligible Inside Resistance

Systems having a high inside conductance (negligible inside heat transfer resistance) combined with a finite but low capacitance are often found in service. The limiting condition of $NTU = \infty$ implies that the capacitance temperature is identical with the gas temperature. This might be the case with the charging or blowdown of a thin walled pressure vessel where jet flow and gas currents create considerable turbulence resulting in high inside conductance values. The following simple model and solutions apply:



$$\text{charging } T^* = \frac{(1 + NTU_\infty - KT_i^* - NTU_\infty T_\infty^*) \left(\frac{C_o^* + 1}{C_o^* + M^*} \right)^{1 + NTU_\infty} + KT_i^* + NTU_\infty T_\infty^*}{1 + NTU_\infty} \quad (8)$$

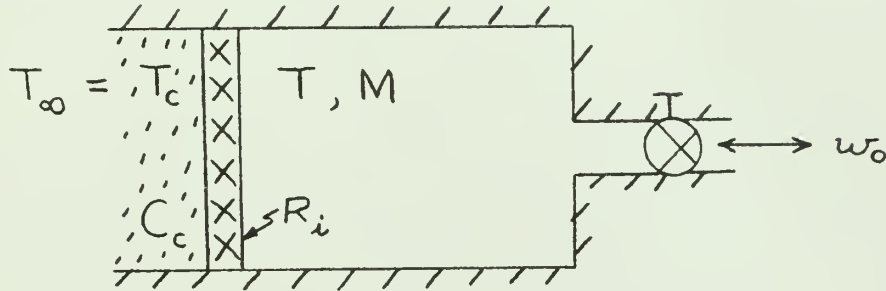
$$\text{blowdown } T^* = \frac{(K - 1 + NTU_\infty - T_\infty^* NTU) \left(\frac{M^* + C_o^*}{1 + C_o^*} \right)^{K - 1 + NTU_\infty} + T_\infty^* NTU_\infty}{K - 1 + NTU_\infty} \quad (9)$$

One real value of these solutions is that they supply definite information for determining the effects of capacitance on the behavior of a system.

5.4. Charging and Blowdown with an Isothermal Sink and Source

In many systems the thermal capacitance of the metal receiver walls far exceeds the thermal capacitance of the gas. In such a case the temperature change of the walls is much less than that of the gas,

and in the limiting case of $C_o^* = \infty$, heat transfer occurs only between an isothermal sink or source and the gas. This might ordinarily be the case with any relatively thick walled receiver or a receiver packed with thermal capacitors. The following simple model and solutions apply:



charging

$$T^* = \frac{kT_i^* + NTU T_c^* - (kT_i^* - 1 - NTU + NTU T_c^*) M^{*-(1+NTU)}}{1 + NTU} \quad (10)$$

blowdown

$$T^* = \frac{(k - 1 + NTU - T_c^* NTU) M^{*k-1+NTU} + T_c^* NTU}{k - 1 + NTU} \quad (11)$$

The value of these solutions is further enhanced in that they can be arranged to give stepwise changes in T^* when the parameters NTU and T_c^* are varying with time.

charging

$$\Delta T^* = \left[\frac{kT_i^* + NTU T_c^*}{1 + NTU} - T^* \right] \left[1 - \left(\frac{M^* + \Delta M^*}{M^*} \right)^{-(1+NTU)} \right] \quad (12)$$

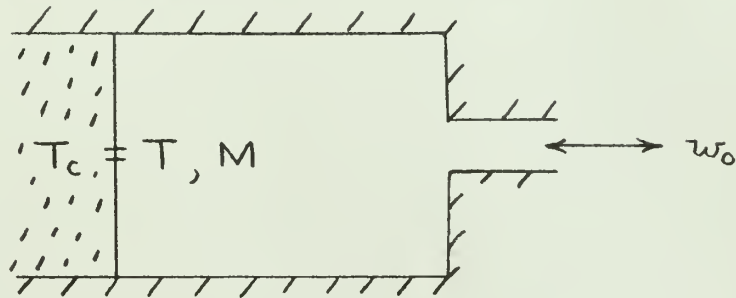
blowdown

$$\Delta T^* = \left[T^* - \frac{NTU}{k - 1 + NTU} T_c^* \right] \left[\left(\frac{M^* + \Delta M^*}{M^*} \right)^{k-1+NTU} - 1 \right] \quad (13)$$

5.5. Isothermal Case

Receivers having a large thermal capacitance accompanied by high

values of inside heat transfer conductance may exhibit essentially isothermal behavior. This might be the case with a blowdown wind tunnel filled with a metal matrix for the purpose of obtaining a near-isothermal blowdown. The effect is to make both C_o^* and NTU very large. The following simple model applies:



The temperature ratio for both charging and blowdown is by definition:

$$T^* = 1 \tag{14}$$

5.6. Application

While it is not true that all engineering systems involving charging or blowdown processes may be treated with these special solutions, many of them will closely fit the limiting conditions. To obtain useful results with these constant resistance solutions, one must use a suitable average NTU. In any real receiver the wide variations in flow rates, temperatures, and pressures will certainly cause considerable variation in heat transfer convective conductance. The remainder of the report will treat in detail the problem of obtaining suitable values of average or time varying conductances for applying these solutions to typical systems. Theoretical considerations of heat transfer conductances will be discussed where directly applicable to the results.

6. Summary of Experimental Results

6.1. Form of Results

Data for all the charging and blowdown runs consisted of tank air temperature and pressure measurements as a function of time. From these data, P^* and T^* were determined from definition and M^* computed from the relationship, $P^* = M^* T^*$ obtained from equation (1). All graphical results are in the form of T^* vs. M^* since T^* is more sensitive than P^* to the effects of heat transfer. Smooth curves were drawn through the plotted data with the comparable theoretical solution indicated by a dashed line. The adiabatic solutions are also shown since any departures from these solutions are an indication of the occurrence of heat transfer.

6.2. Uninsulated Tank

A series of constant flow charging and blowdown runs were conducted with the uninsulated tank in the "as found" condition with no additional heat capacitors. The capacitance of the tank walls was of sufficient magnitude that heat transfer essentially occurred to and from an isothermal sink and source. The following runs were conducted:

TABLE 2

<u>Summary of Uninsulated Tank Runs</u>						
<u>Run No.</u>	<u>Type</u>	<u>Orifice Dia. (in)</u>	<u>w_o (lbs/hr)</u>	<u>t (sec)</u>	<u>C_o^*</u>	<u>NTU</u>
1	Charge	1/8	180	200	300	10.5
2	Charge	3/16	380	100	300	7.5
3	Charge	1/4	711	55	300	5.7
4	Charge	5/16	1140	35	300	4.1
5	Blow	3/16	105	240	41	5.0
6	Blow	1/4	166	140	41	3.5
7	Blow	5/16	257	80	41	2.9
8	Blow	3/8	375	70	41	2.6

The test results are presented in Tables 11 and 12 of Appendix IV and are shown graphically on Figs. 5, 6, and 7. Solutions based upon equations (10) and (11) to fit the experimental results are shown graphically for comparison. The values of NTU listed in Table 2, page 15, are those used in these equations. The values of C_0^* were obtained directly from equation (5) based on a wall thermal capacitance of $C_0 = 92 \text{ Btu/}^\circ\text{R}$.

6.3. Insulated Tank

Several charging and blowdown runs were made with the insulated tank without added heat capacitors in order to attain, as nearly as possible, an adiabatic process and to gage the effectiveness of the insulation. The following runs were conducted:

TABLE 3

Summary of Insulated Tank Runs

<u>Run No.</u>	<u>Type</u>	<u>Orifice Dia. (in)</u>	<u>w_0 (lb/hr)</u>	<u>t (sec)</u>
9	Charge	5/16	1130	20
10	Charge	3/8	1320	16
11	Charge	7/16	1960	11
12	Blow	1/4	395	120
13	Blow	3/8	841	40
14	Blow	7/16	860	35
15	Blow	1/2	1100	26

The test results are presented in Tables 13 and 14 of Appendix IV and are shown graphically on Figs. 8 and 9. The adiabatic solutions from equations (6) and (7) are shown for comparison.

6.4. Insulated Tank with Added Heat Capacitors

A series of constant mass flow charging and blowdown runs were made with a set of vertical strip aluminum heat capacitors inserted in the

insulated tank. Capacitor configuration and air flow rates were selected such that the air temperature closely followed that of the capacitance for the case of heat transfer with negligible inside resistance. The following runs were conducted:

TABLE 4
Summary of Insulated Tank Runs
with Added Capacitors

<u>Run No.</u>	<u>Type</u>	<u>Orifice Dia. (in)</u>	<u>w_o (lb/hr)</u>	<u>t (sec)</u>	<u>C_o^*</u>
16	Charge	3/16	407	70	10.0
17	Charge	1/4	704	40	10.0
18	Charge	5/16	1104	25	10.0
19	Blow	5/16	255	70	1.44
20	Blow	3/8	356	50	1.44
21	Blow	7/16	497	35	1.44

The test results are presented in Tables 15 and 16 of Appendix IV and are shown graphically on Figs. 10 and 11. Solutions based on equations (8) and (9) to fit the experimental results are shown graphically for comparison. The values of C_o^* were obtained directly from equation (5) based on a thermal capacitance of $C_c = 2.2 \text{ Btu/}^\circ\text{R}$.

7. Discussion of Results

7.1. Uninsulated Tank

7.1.1. General

Several charging and blowdown runs, as listed in Table 2, page 15, were made with the uninsulated tank in the "as found" condition with no additional heat transfer surfaces. The tank was selected as a typical medium pressure air receiver of the type utilized for compressed air systems. The cylindrical tank walls and dished heads were constructed of 1/2-in. steel plate having a total thermal capacitance of $C_c = 92.0 \text{ BTU/}^\circ\text{R}$.

7.1.2. Charging of Uninsulated Tank

The mass of air in the tank prior to charging was $M_0 = 1.8 \text{ lbs.}$ for all runs, giving a value of $C_0^* = 300$ from equation (5). This value is well above the figure of $C_0^* = 40$ recommended by Reynolds [2] as the minimum for infinite capacitance behavior. Therefore, the solution for charging with heat transfer to an isothermal sink would be expected to apply. The capacitance temperature during all charging runs remained essentially constant at $533 \text{ }^\circ\text{R}$ giving a value of $T_c^* = 0.995$. Charging air entered at a constant mass flow rate at a temperature of $531 \text{ }^\circ\text{R}$ giving a value of $T_1^* = 0.990$. Inserting these constant values in equation (10) together with the best value of NTU fitting the experimental points, resulted in the solutions of T^* vs. M^* shown graphically on Fig. 5. For values of $M^* > 3$ it was found that equation (10) yields a constant value of T^* . Inspection of the experimental data shows that for all runs a constant value of T^* was attained after about 35 seconds. The values of NTU used in

equation (10) were therefore selected to give a calculated T^* coinciding with these constant experimental values.

A convective heat transfer conductance, h , can be found from the definition:

$$NTU = \frac{(h A)_i}{w_o c_v}$$

If the best single value of NTU fitting the experimental points is substituted in this definition, the resulting value of conductance, h , becomes a mean convective conductance, h_m , implied constant over the entire charging run. Values of h_m from NTU are listed in Table 5 below.

TABLE 5
Charging Conductances
Uninsulated Tank

Run No.	w_o (lb/hr)	NTU (Eqn.10)	h_m (from NTU) (Btu/hrft ²⁰ R)	max. h_{ave} (free cony.) (Btu/hrft ²⁰ R)	max. h_{ave} (pred. Fig.12) (Btu/hrft ²⁰ R)
1	180	10.5	7.2	2.1	7.7
2	380	7.5	10.7	2.5	11.0
3	711	5.7	15.0	2.7	14.0
4	1140	4.1	17.5	2.9	16.5

If the mechanism of heat transfer between the air in the tank and the tank walls is simple free convection, McAdams [5] recommends as a correlation

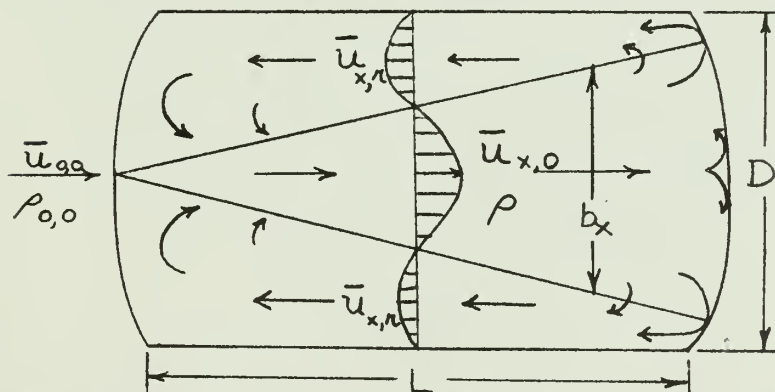
$$h_{ave} = \frac{K}{L} 0.13 (Gr Pr)^{1/3} \quad (15)$$

for $10^{10} < Gr Pr < 10^{11}$. Inserting in equation (15) the maximum value of temperature attained during each run results in the maximum values of average convective heat transfer conductance, h_{ave} , listed in Table 5. Since these conductances are considerably lower than those calculated from NTU, it is therefore concluded that the heat transfer mechanism for

charging is forced convection. It is also apparent that the conductances vary with time since the experimental values of T^* decrease after attaining an initial peak value. This bears out the observation of Reynolds [2] that in any real receiver the wide variations in temperature and pressure would cause considerable variation in the heat transfer convective conductance.

The presence of forced convection considerably compounds the problem of predicting heat transfer conductances. There is inevitably present a jet of fluid discharging through the orifice into a region of increasing pressure. While no analytical treatment of this specific problem has been found, there is considerable information available concerning the behavior of free jets discharging into a region of fluid at rest. Theory concerning the transport of momentum in an isothermal, turbulent, free jet of air discharging at subsonic velocities into air at the same density might be expected to lead to useful results in the present problem.

Therefore, let us consider the following to be a simplified model of the jet and resulting flow inside the tank:



Considering the jet as originating from a point at the orifice, observations show that such a jet spreads out conically with a width b

directly proportional to the distance x from the origin [6]. The cone angle has been found to be about 25° [7] independent of the velocity at the origin, $\bar{u}_{0,0}$. As the jet advances, the maximum velocity, $\bar{u}_{x,0}$, at a point x on the centerline diminishes proportional to $1/x$ [8]. Fresh masses of fluid are continually being drawn in so that the mass flow at succeeding cross sections is not the same. The jet momentum, however, is constant since the pressure is assumed the same as that of the surrounding fluid [8]. These relationships may be expressed as follows:

$$b \sim x \quad (16)$$

$$\bar{u}_{x,0} \sim \frac{1}{x} \quad (17)$$

$$I = \rho \bar{u}_{x,0}^2 \pi b^2 \cdot \text{const} \quad (18)$$

These relationships have been combined and experimentally verified by Alexander, et al., [9] in the form of momentum flux ratios expressible in terms of the ratio of orifice diameter to the distance x , as follows:

$$\frac{(\rho \bar{u}^2)_{x,0}}{(\rho \bar{u}^2)_{0,0}} = \left(\frac{d}{Kx} \right)^2 \quad (19)$$

where K is a constant experimentally determined for various initial velocities. Since the orifice discharge region pressure is always less than the critical pressure, the air will have expanded at the orifice throat only to the critical pressure. Therefore the quantity $(\rho \bar{u}^2)_{0,0}$ will be a constant independent of orifice size during constant flow charging. Equation (19) may be placed in the form,

$$\bar{u}_{x,0} = \frac{\sqrt{(\rho \bar{u}^2)_{0,0}} d}{\rho^{1/2} K x} = \frac{C}{\rho^{1/2} x} \quad (20)$$

where ρ is now dependent only on the tank pressure and temperature, assumed constant throughout the tank. From the familiar critical flow metering equation and from continuity, an average discharge velocity was found to be 1050 ft/sec. At this velocity, Alexander [9] recommends $K=0.134$, giving the following values of C from equation (20),

<u>d (in.)</u>	<u>C (ft lb)^{1/2}/Sec</u>
1/8	750
3/16	1125
1/4	1500
5/16	1690

from which $\bar{u}_{x,0}$ may be found at any point along the jet axis.

Now consider the jet as impinging upon the dished head of the tank and being deflected, as shown in the model, down along the walls in a concentric annulus. If this be the case, then in order that there be no pressure difference throughout the tank, the mass flow upwards in the jet must equal the mass flow down through the outer annulus at any cross section. From continuity, the average velocity in the outer annulus at any distance x in terms of the annular and jet areas is

$$\bar{u}_{x,r} = \frac{A_{x,0}}{A_{x,r}} \bar{u}_{x,0} \quad (21)$$

For turbulent flow in concentric annuli, McAdams [5] recommends for the local convective heat transfer conductance,

$$h_x = .023 \frac{c_p G}{(Pr)^{2/3} (Re)^{.2}} \quad (22)$$

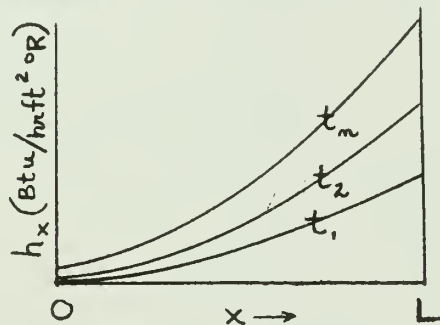
where Re is based on the equivalent diameter,

$$D_x = D - b_x \quad (23)$$

Substituting equations (20) and (21) in equation (22) and using average values for the Prandtl number gives

$$h_x = 2.6 \left(\frac{\rho}{\sqrt{D_x}} \right)^{.4} \left(\frac{A_{x,o}}{A_{x,r}} \cdot \frac{C}{x} \right)^{.8} \quad (22a)$$

Equation (22a) was used to calculate the local convective conductance, h_x , at equally spaced intervals along the walls at various time intervals for each charging run using the experimental pressure-temperature data to evaluate the density. Thus for each run a series of curves of the type shown below were plotted. These curves show a



decreasing local conductance, tank top to bottom. From these curves, an average convective heat transfer conductance, h_{ave} , was determined for each time increment. Values of h_{ave} are shown graphically on Fig.(12). In all cases the predicted h_{ave} was found to have occurred at a point about $\frac{1}{2}$ the total tank height. For comparison, equation (10) was solved for an NTU corresponding to each experimental T^* vs. M^* point. Using these values of NTU, an experimental h_{ave} was calculated from the definition of NTU for each experimental point. These experimental values of h_{ave} are also shown on Fig. (12).

Comparison of the curves on Fig. (12) shows a good correlation between the predicted h_{ave} and that determined from the experimental points. As expected, increases in pressure and density predominate at the higher flow rates giving increased convective conductances and an increased NTU. The predicted values of h_{ave} follow the trend of the experimental values extremely well although lagging somewhat in magnitude. At the lower flow rates the average convective conductance remains almost constant and this trend is not predicted as well by equation (22a). At such flow rates, however, the process is essentially isothermal and therefore the simple relationship $T^* = 1$ gives adequate results. At the higher flow rates where NTU is changing with time equation (22a) can be used to predict NTU for use in stepwise equation (12) with results at least adequate for design and certainly better than would be predicted from adiabatic behavior.

7.1.3. Blowdown of Uninsulated Tank

The mass of air in the tank prior to blowdown was $M_0 = 13.2$ lbs. for all runs yielding a value of $C_0^* = 41$ from equation (5). This is well above the value of $C_0^* = 6.5$ recommended by Reynolds [2] as a minimum for infinite capacitance blowdown. Therefore, the solution for blowdown with heat transfer from an isothermal source would be expected to apply. The capacitance temperature during all blowdown runs remained essentially constant at $535^\circ R$. Solutions of T^* vs. M^* based on equation (11) are shown graphically on Fig. 6 and 7 for the best value of NTU fitting the experimental points.

Once again, solving for the mean heat transfer conductance over the entire run, h_m , from the definition of NTU yields the values listed in Table 6.

TABLE 6

Blowdown Conductances
Uninsulated Tank

Run No.	w_o (lb/hr)	NTU (Eq. 11)	h_m (from NTU) (Btu/hrft ² °R)	h_m (free cony.) (Btu/hrft ² °R)	% Difference
5	105	5.0	1.96	1.80	8
6	166	3.5	2.16	1.85	14
7	257	2.9	2.79	1.90	32
8	375	2.6	3.65	1.90	49

It is now of interest to compare the test results with conductances predicted on the basis of an assumption of a steady state turbulent free convection boundary layer over the entire heating surface. If average properties of air are inserted in equation (15), but the pressure dependence of the density retained, we obtain the equation for an average convective conductance,

$$h_{ave} = .038 (P^2 \Delta T)^{1/3} \quad (15a)$$

where P is the pressure in psia and ΔT is the temperature difference between the air and the tank walls in °F. Representative results from this equation for runs 5 and 6 are plotted on Fig. 13. In all cases the conductance drops sharply to zero when the air temperature reaches that of the tank wall and then rises rapidly to remain relatively constant over the remainder of the run. The mean predicted conductances with time from these curves are shown in Table 6 above.

In each case, the predicted mean conductances are less than the measured mean conductances. At the slower flow rates the per cent difference is reasonably small considering the inherent uncertainty in

matching the analytical curves and the experimental data. Reynolds [3] found differences of the same order of magnitude for similar blowdowns at critical flow. Runs 7 and 8, however, show that this difference becomes more pronounced as the flow rate increases. Steady state conditions still seem to persist since the experimental points for these runs (Fig. 7) follow the theoretical curves down to a point where constant flow departure begins. Large flow rates, however, yield small values of NTU and a closer approach to adiabatic behavior (Fig. 7) so that the precise evaluation of conductance might not be required. If, as Reynolds [3] points out, it is the relatively slow blowdown process that provides the most difficulty for the engineer because of heat transfer, then for such cases steady-state heat transfer correlations apparently provide a good approximation.

Blowdown systems where the evaluation of forced convection conductances becomes important are common enough. Murphy [1] found that for a blowdown wind tunnel with added heat capacitors, heat transfer occurred at a rate of about eight times that predicted for free convection. This system differed from the simple case considered here in that capacitors were installed in a section separate from the air receiver, through which the air passed during blowdown and charging. Evaluation of forced convection conductance, therefore, would be dependent upon design characteristics and presumably predictable from available theory.

For a tank of dimensions similar to the one used in these experiments, it is probable that the blowdown heat transfer mechanism would be free convection. Thus the relationships similar to equation (15) would give good approximations especially if increased slightly by

good judgment to allow for some forced convection effects at higher flow rates.

7.2. Insulated Tank

7.2.1. General

Several charging and blowdown runs, as listed in Table 3, page 16, were conducted with the insulated tank in order to determine how closely the adiabatic solutions would apply to a system deliberately insulated from the containing walls. Choice of an insulation material presented a compromise of several considerations. Ideally, a material with both a low diffusivity ($k/\rho c_p$) and low thermal storage capacity (ρc_p) is required in order to have the surface temperature follow that of the air while the change of energy storage remains small. Inasmuch as the tank was relatively large in size, a material of sufficient structural rigidity was also needed for ease of installation and dimensional stability under pressure. Foamed polystyrene insulation (Dow Chemical Styrofoam, HD2) was first selected and installed in the tank. This material, although possessing both a low diffusivity and low energy storage capacity, buckled under a hydrostatic pressure of 50 psig and came loose from the tank walls. This relatively low pressure also reduced the thickness of the Styrofoam about 10 percent. Therefore, redwood was selected as the most economical alternative material despite a relatively high density (25 lbs/ft^3) and resulting high thermal storage capacity.

7.2.2. Charging of Insulated Tank

Reynolds [2] predicts that the adiabatic charging solution should be applicable for values of $NTU < 0.25$ for all magnitudes of C_o^* . From

equation (3) it is seen that a low NTU for a given area is attained by the combination of a high initial flow rate and a low heat transfer conductance. Therefore, orifice plates were selected to give the highest flow rate possible within a reasonable charging time. The results of the three runs, as displayed on Fig. 8, show considerable departure from the adiabatic solution.

Inasmuch as the flow rates and areas are fixed, let us consider the magnitude of the mean convective heat transfer conductance, h_m , required to give a maximum NTU = 0.25. Solving for h_m from the definition of NTU yields the conductance values listed in Table 7.

TABLE 7

Charging Conductances - Insulated Tank

<u>Run No.</u>	<u>w (lb/hr)</u>	<u>max. h_m (for NTU = 0.25) (Btu/hr ft²°R)</u>
9	1130	1.26
10	1320	1.48
11	1960	2.19

It was seen, however, from the uninsulated tank results of Table 5, p. 19, that the conductances are in reality an order of magnitude greater than the above maximum values. This would then give a corresponding value of NTU = 2.5. Even though Fig. 8 shows a nearer approach to the adiabatic line for the fastest run, it is conceivable that at faster charges the heat transfer conductances would increase to such an extent as to cause a departure from rather than a continual approach to the line.

Reference [2] also gives as a criterion for adiabatic charging

the condition of $C_0^* < 0.04$ for NTU reasonably low. Even if NTU = 2.5 is reasonably small, it will be shown in the next section that the C_0^* of the insulation increases with time to values considerably in excess of the maximum $C_0^* = 0.04$. This low value of C_0^* is unrealistic at best since its attainment would require a capacitance in this case of only $C_c = 0.086$ Btu/°R (equation (5) with $M_0 = 12.8$ lb), a low value for the best of insulation.

Thus it would seem that the criteria of NTU < 0.25 , although well within the range of free convection heat transfer conductances, is unattainable with a tank where the charging jet effect raises the conductance materially. As a result, it was not possible to attain a small enough NTU, while charging the insulated tank, to evaluate fully the limiting conditions for adiabatic charging.

7.2.3. Blowdown of Insulated Tank

For the case of adiabatic blowdown, Reynolds [2] limits the conditions to NTU < 0.08 for all magnitudes of C_0^* . As in the case of charging, small values of NTU were sought by increasing the flow rate. Therefore, all blowdown runs were made at critical mass flow in order to attain the greatest value of initial flow rate. These runs are summarized in Table 3, page 16, and shown graphically on Fig. 9. As in the case of charging, Fig. 9 shows a considerable departure from adiabatic behavior. If once again we solve for the mean convective heat transfer conductance, h_m , from the limiting value of NTU = 0.08, we obtain the values listed in Table 8, page 30.

Results previously obtained from blowdown runs conducted with the insulated tank (Table 6, page 25) indicate that conductances slightly

TABLE 8

Blowdown Conductances
Insulated Tank

<u>Run No.</u>	<u>w₀</u> <u>(lbs/hr)</u>	<u>max. h_m</u> <u>(Btu/hr ft²°R)</u>
12	395	0.14
13	841	0.30
14	860	0.31
15	1100	0.29

greater than those predicted for free convection might be expected. Inasmuch as these free convection conductances are an order of magnitude greater than the values of h_m listed in Table 8, the actual NTU for blowdown of the insulated tank is considerably greater than the value of $NTU = 0.08$.

Several phenomena of interest are deducible from Fig. 9. It is noted that run 12, although at a slower flow rate and presumably at a higher NTU than the other runs, approaches the adiabatic line early in the run. This might be explained qualitatively by considering the test procedure. Blowdown was started immediately after charging and thus the air was at a relatively high temperature while the insulation remained essentially at ambient. Therefore, for a long blowdown there was time for considerable heat transfer to such an isothermal sink, dropping the temperature appreciably. At the end of the run conditions were reversed. The insulation now acted as an isothermal source for heat transfer from the lower temperature air. Thus toward the end of the run the air temperature dropped less rapidly. (This effect is also quite apparent with blowdown runs 5 and 6, Fig. 6, conducted with the uninsulated tank.)

As flow rates increase and the run time decreases, this "apparent adiabatic" effect becomes less pronounced and, in the case of run 13, the temperature drop appears more nearly linear and departs further from adiabatic. As the flow rate increases further this linearity is more apparent and, since NTU decreases, the behavior again approaches adiabatic as seen by run 14. A still further increase in flow rate as with run 15 might be expected to further approach the adiabatic line, but this was not the case. Here, it is probable that h was also increasing due to increased convection, thus offsetting the increase in w_0 and in effect increasing NTU. Thus it would appear that a limiting approach to adiabatic behavior is all that may be attained within reasonable blowdown times with an arrangement such as this.

Again, Reynolds [2] establishes the condition of $C_0^* < 0.04$ and NTU reasonably small as a criterion for adiabatic behavior. These conditions might conceivably become more realistic for blowdown than for charging since the initial mass of air in the tank is considerably greater than for charging and NTU small in comparison. In this case, an $M_0 = 8.8$ lbs. yields a $C_c = 0.06$ Btu/ $^{\circ}$ R, a small value considering the capacity of the redwood insulation for storage of energy.

7.3. Added Heat Capacitors in Insulated Tank

7.3.1. General

Several charging and blowdown runs, as listed in Table 4, page 17, were conducted with added heat capacitors inserted in the insulated tank. The insulated tank was used in order to eliminate heat transfer from outside the receiver ($NTU_{\infty} = 0$) and to minimize the effects of the tank walls so that most of the heating surface would be the heat

capacitors. Sixteen 0.012 in. thick aluminum strip capacitors, each 12 in. by 40 in., were installed in a vertical and radial position in the tank and spaced evenly in order to interfere as little as possible with the air flow patterns previously discussed. The surface area of the capacitors was 108 ft² increasing the total area, including the tank walls, to 146 ft². Total weight of the capacitors was 10.0 lbs. Thus the primary effect of the capacitance was to increase the heat transfer area and, therefore, NTU.

7.3.2. Charging of Insulated Tank with Added Capacitors

The mass of air in the tank prior to charging was $M_0 = 1.3$ lbs., yielding a value of $G_0^* = 10.0$ from equation (5). Inasmuch as this value of G_0^* is considerably lower than the minimum of $G_0^* = 40$ recommended for infinite capacitance behavior [2], it is necessary now to estimate NTU. Since an approximation is justifiable, the conductance results previously obtained with the uninsulated tank were used. Insertion of the minimum experimental values of average conductance from Fig. 12 in the definition of NTU yields the values of NTU listed in Table 9 below.

TABLE 9

Charging Conductances
Added Capacitors in Insulated Tank

<u>Run No.</u>	<u>w_0 (lb/hr)</u>	<u>min. h_{ave} (Fig. 12) (Btu/hrft²°R)</u>	<u>NTU (Eq. 3)</u>	<u>G_0^*</u>
16	407	8.0	16.9	10.0
17	714	10.3	12.6	10.0
18	1104	12.0	9.4	10.0

These values are each above the minimum value of $NTU > 7$ recommended by Reynolds [2] for infinite NTU behavior. Inasmuch as the temperature of

the capacitance closely followed that of the air, the solution for negligible inside resistance would be expected to apply.

If $NTU = 0$ and $T_1^* = 1$, equation (8) reduces to:

$$T^* = 1.4 - 0.4 \left(\frac{C_o^*}{C_o^* + M^*} \right) \quad (8a)$$

Equation (8a) solved for $C_o^* = 10.0$ is shown graphically on Fig. 10. Comparison of this curve with the experimental mean plot shows a considerable variance. Inasmuch as equation (8a) is independent of a heat transfer rate (i.e. $NTU_{\infty} = 0$), it is also independent of mass flow rate and all runs should follow the same curve. There is some variance here as seen in Fig. 10.

Since equation (8a) is sensitive to small changes in C_o^* , any increase in receiver capacitance, C_o , with time would considerably affect T^* . This is especially true since the initial capacitance of the air ($M_o c_v$) is relatively small. As was seen from the insulated tank runs without heat capacitors (Fig. 5), there is considerable heat transfer to the insulation during a typical charge. Therefore, a comparison of the increase in insulation C_o^* alone during a run with that given by equation (8a) for the experimental data should give an indication of the applicability of this solution.

The temperature distribution in the redwood as a function of time was calculated by the Schmidt graphical method [10] for run 17, selected as representative. The plot was based upon a thermal diffusivity of $0.004 \text{ ft}^2/\text{hr}$ and an average surface conductance of $14 \text{ Btu}/(\text{hrft}^2\text{R})$ from the uninsulated tank results. The results of the graphical solution are shown in Fig. 14a. The capacitance at the end of each time interval was calculated from the relationship,

$$Q_s = C_c \Delta T \quad (24)$$

Where Q_s is the heat stored in redwood as calculated from the internal temperature differences and ΔT is the difference between the tank air and ambient temperatures. The resulting increase in insulation C_0^* with time is shown as curve (1) on Fig. 14b. Next, values of C_0^* for the liner plus the capacitors were calculated from equation (8a) at each time interval using experimental values of T^* and M^* . These are shown as curve (2) on Fig. 14b. The increasing values of C_0^* for the liner alone were then subtracted from the experimental values of C_0^* for the liner plus the capacitors, resulting in curve (3). This curve is essentially constant at $C_0^* = 10.0$ and thus is in agreement with the measured value for the added capacitors independent of the insulation.

Similar treatment of the other charging runs would be expected to yield the same results. Scatter of the experimental data may be attributed to variances in conductance, the smaller flow rates showing less effects of heat transfer to the insulation. It is seen then that equation (8) gives good results for the case where the capacitance temperature follows that of the gas. For the more general application where external heat transfer ($NTU \neq 0$) enters, the determination of natural convection conductances for the external tank and ambient air should present no problem.

7.3.3. Blowdown of Insulated Tank with Added Capacitors

The mass of air in the tank prior to blowdown was $M_0 = 9.0$ lbs., resulting in $C_0^* = 1.44$ from equation (5). This value is much lower than the infinite capacitance value of $C_0^* = 6.5$. As with charging, the values of NTU listed in Table 10 have been estimated from the results listed in Table 6, p. 25, for the uninsulated tank.

TABLE 10

Blowdown Conductances
Added Capacitors in Insulated Tank

<u>Run No.</u>	<u>w_o</u> <u>(lbs/hr)</u>	<u>h_m</u> <u>(Btu/hr ft²°R)</u>	<u>NTU</u> <u>(Eqn. 3)</u>	<u>C_o[*]</u>
19	2551	2.9	8.6	1.44
20	356	3.6	8.7	1.44
21	497	4.4	7.6	1.44

Since the NTU values are each above the minimum value of NTU > 7.5 recommended by Reynolds [2] and since the capacitance temperature closely followed that of the air, the solutions for negligible inside resistance should apply. If NTU_∞ = 0 and T₁^{*} = 1, equation (9) reduces to:

$$T^* = \left(\frac{M^* + C_o^*}{1 + C_o^*} \right)^{0.4} \quad (9a)$$

The solution of equation (9a) for C_o^{*} = 1.44 is shown graphically on Fig. 11. The curve follows the experimental points quite well for the higher flow rates with a gradual departure toward the end of the run. As in charging, the system capacitance ratio, C_o^{*}, would be expected to increase with time due to heat transfer with the insulation. Such a change would be characterized by lower values of T^{*} with time. In blowdown, however, the initial capacitance of the air (M_o cv) is much larger than for charging. Thus slight increases in C_o with time would have considerably less effect for blowdown than for charging. Relatively fast blowdown runs were made in order to minimize the heat transfer with the insulation and, as shown on Fig. 11, the fastest run (run 21) follows best the theoretical curve.

It would be expected that the slower runs would lie above this

curve in a region of increased C_0^* (lower T^*). That this is not the case is shown by run 19. Since the heat transfer conductances are much smaller for blowdown than for charging, the insulation surface temperature does not follow that of the air and as a result the insulation acts much as an isothermal sink and source. Thus the slower runs appear similar to run 12 shown on Fig. 9 with the same behavior as discussed previously. All runs, however, exhibit the effect of heat transfer from the higher temperature insulation to the lower temperature air.

Despite the anomalies introduced by the insulation, it would appear that the blowdown solution for negligible internal resistance yields reliable predictions for system behavior where the capacitance temperature follows that of the gas. As with charging, the introduction of external heat transfer should present no problem in the determination of heat transfer conductances.

7.4. Mixing Considerations

As stated previously, the derivations of the solutions evaluated in this report are based upon the assumption that the gas temperature is uniform throughout the tank at any given time. This assumes that during charging the incoming gas expands and diffuses instantaneously throughout the gas in the receiver. Therefore, it was considered expedient to perform an experiment during a representative charging run to determine the validity of this assumption. The test apparatus was so arranged (Fig. 2) that the four air temperature thermocouples could be monitored individually during a run. Run 4, selected as representative, was repeated under identical conditions, each time recording the output of a different thermocouple. The temperatures so obtained revealed no variance greater than 0.5 °F. This was indeed the expected result considering the mixing potential of the jet flow described earlier.

This is, however, contrary to findings briefly referred to by Reynolds [2] to the effect that considerable temperature gradients existed throughout a charging run. Although the geometry of the receiver was not described, such results might be attained with a tank where the charging jet cone diameter exceeds that of the tank. Such an arrangement might conceivably result in a piston effect causing temperature gradients between upper and lower layers of gas in the tank.

8. Conclusions

The conclusions to be drawn from this investigation are summarized as follows:

- (a) Excellent quantitative agreement between the experimental results and the simplified analytical solutions of Reynolds [2] have been obtained for both charging and blowdown.
- (b) Constant mass charging directly through an orifice into the bottom of a receiver of sufficient diameter for the formation of a freely expanding fluid jet results in forced convection heat transfer conductances between the air and the tank walls. These conductances increase as the air temperature and pressure change with time and vary in magnitude over the interior surface.
- (c) During relatively slow constant mass flow blowdowns, the heat transfer conductances tend to be constant and a time average free convection conductance gives a satisfactory approximation for a large capacitance system. This method becomes less reliable as the flow rate increases and a more detailed analysis, related to the geometry of the system, would be required.
- (d) Analytical expressions have been found to predict forced convection conductances during charging that closely approximate the experimental values. At relatively high mass flow rates, these expressions can be used with available stepwise solutions as a basis for preliminary design of high capacitance systems. At relatively low mass flow rates, the conductances are of sufficient magnitude to give essentially isothermal behavior.
- (e) Despite the high mass flow rates possible with a relatively large size air receiver, it is unlikely that an adiabatic charging process

would ever be attained within a reasonable charging time in the presence of a jet effect forced convection heat transfer mechanism.

(f) Closer approach to adiabatic behavior is attained during blowdown than during charging for the same constant flow rate. An approach limit is reached for blowdown, however, since even though the flow rate is increasing the heat transfer conductance is also increasing until the effect of the latter exceeds that of the former.

(g) If the reservoir is of sufficient diameter for the formation of a fully expanding fluid jet during charging, there will be adequate mixing with no temperature gradient in the receiver.

9. Recommendations

It is recommended that the general problem of charging and blowdown be analysed for solution by analog computer methods. Despite the problems encountered with the simplified computer setup evaluated in Appendix III, it is considered that the general problem of charging and blowdown is inherently suitable to treatment by such methods.

BIBLIOGRAPHY

1. J. S. Murphy, D. Rennie, and G. W. Timson, Stagnation Temperature Control in Blowdown Wind Tunnels, *Journal of the Aero Space Sciences*, Vol. 25, No. 11, November, 1958, pp. 69-698.
2. W. C. Reynolds, An Analytical Investigation of the Blowdown and charging Processes in a Single Gas Receiver, Including the Effects of Heat Transfer, Stanford Tech. Report T-1, October 1, 1955.
3. W. C. Reynolds, J. W. Millard, W. M. Kays, An Experimental Investigation of the Blowdown Process in a Single Gas Receiver, Including the Effects of Heat Transfer, Stanford Tech. Report T-2, December 1, 1956.
4. F. D. Wener, The Design of Diaphragms for Pressure Gages Which Use the Bonded Wire Resistance Strain Gage, *Proceedings of the Society for Experimental Stress Analysis*, Vol. XI, No. 1, 1953.
5. W. H. McAdams, *Heat Transmission*, 3rd Ed., McGraw-Hill Book Co., 1954.
6. H. Schlichting, *Boundary Layer Theory*, McGraw-Hill Book Co., 1955.
7. J. O. Hinze and B. G. Van Der Hegge Zijnen, Transfer of Heat and Matter in the Turbulent Mixing Zone of an Axially Symmetrical Jet, *Applied Scientific Research*, Vol. A1, No. 5-6, 1949.
8. L. Prandtl, *Essentials of Fluid Dynamics*, Hafner Publishing Co., 1949.
9. L. G. Alexander, T. Baron, and E. W. Comings, Transport of Momentum, Mass, and Heat in Turbulent Jets, *University of Michigan Bulletin*, Vol. 50, No. 66, May 1953.
10. W. H. Giedt, *Principles of Engineering Heat Transfer*, D. Van Nostrand Co., Inc., 1957.
11. G. A. Korn and T. M. Korn, *Electronic Analog Computers*, 2nd Ed., McGraw Hill Book Co., 1956.

APPENDIX I

Derivation of Charging and Blowdown Solutions

APPENDIX I

Derivation of Charging and Blowdown Solutions

1. Equations of State

In all of the analyses to follow, the working fluid is presumed to be a perfect gas, with constant specific heats, having the following equations of state:

$$P V = (R/m) T$$

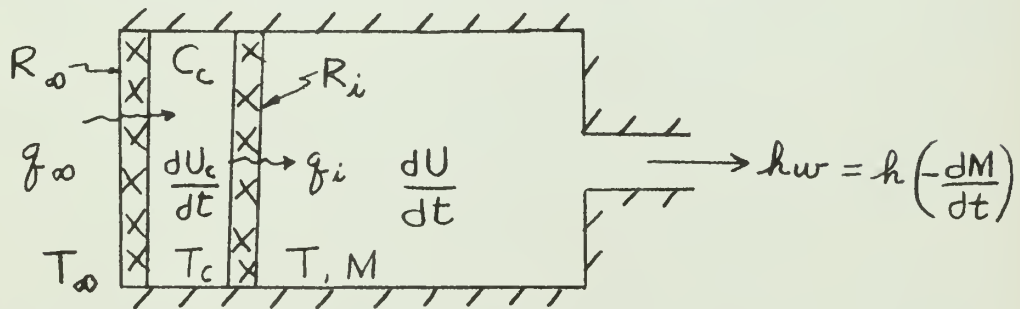
$$u = c_v T$$

$$h = c_p T$$

$$k = c_p / c_v$$

$$(R/m) = c_p - c_v$$

2. General Differential Equation for Blowdown and Charging



An energy balance for the gas in the receiver gives:

$$\frac{dU}{dt} = g_i + h \frac{dM}{dt}$$

An energy balance on the capacitance gives:

$$g_\infty - g_i = \frac{dU_c}{dt}$$

Rate equations for the two heat transfer resistances give:

$$g_\infty = \frac{T_\infty - T_c}{R_\infty} \quad \text{and} \quad g_i = \frac{T_c - T}{R_i}$$

The change in energy storage in the gas due to mass flow out and changes in specific energy is:

$$\frac{dU}{dt} = \frac{d(Mu)}{dt} = M \frac{du}{dt} + u \frac{dM}{dt}$$

Assuming the specific heat of the capacitance is constant, the change in energy storage in the capacitance is:

$$\frac{dU_c}{dt} = C_c \frac{dT_c}{dt}$$

Combining the energy balances, rate equations, and the perfect gas equations of state:

$$M \frac{dT}{dt} = (k-1)T \frac{dM}{dt} + \frac{T_c - T}{R_i C_v}$$

$$\text{and } \frac{dT_c}{dt} = \frac{T}{R_i C_c} - \left[\frac{1}{R_\infty C_c} + \frac{1}{R_i C_c} \right] T_c + \frac{T_\infty}{R_\infty C_c}$$

Now since $w = \frac{dM}{dt}$, then:

$$\frac{dT}{dt} = \frac{dT}{dM} \frac{dM}{dt} = w \frac{dT}{dM} \quad \text{and} \quad \frac{dT_c}{dt} = \frac{dT_c}{dM} \frac{dM}{dt} = -w \frac{dT_c}{dM}$$

Thus inserting these relationships we may write:

$$M \frac{dT}{dM} - \left[(k-1) + \frac{1}{R_i C_v w} \right] T + \frac{1}{R_i C_v w} T_c = 0$$

$$\text{and } \frac{dT_c}{dM} - \frac{1}{C_c} \left[\frac{1}{R_\infty w} + \frac{1}{R_i w} \right] T_c + \frac{T}{R_i C_c w} + \frac{T_\infty}{R_\infty C_c w} = 0$$

These equations expressed in terms of dimensionless parameters become:

$$w^* M^* \frac{dT^*}{dM^*} - \left[(k-1)w^* + NTU \right] T^* + NTU T_c^* = 0$$

$$\text{and } w^* \frac{dT_c^*}{dM^*} - \frac{1}{C_o^*} \left[NTU_\infty + NTU \right] T_c^* + \frac{1}{C_o^*} NTU T^* + \frac{1}{C_o^*} NTU_\infty T_\infty^* = 0$$

These may be combined into a single equation expressed as follows:

$$w^{*2} M^* \frac{d^2 T^*}{dM^{*2}} + w^* \left\{ M^* \frac{dw^*}{dM^*} + w^* (2-k) - NTU - \frac{M^*}{C_o^*} (NTU + NTU_\infty) \right\} \frac{dT^*}{dM^*} + \frac{1}{C_o^*} \left\{ (k-1)w^* (NTU + NTU_\infty) + NTU NTU_\infty - w^* (k-1) \frac{dw^*}{dM^*} \right\} T^* - \frac{NTU NTU_\infty}{C_o^*} T_\infty^* = 0$$

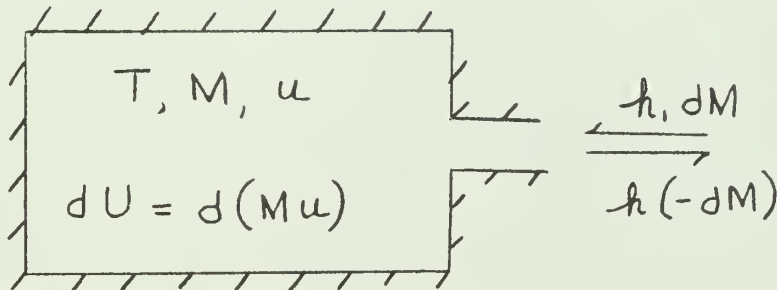
For constant mass flow, $w^* = 1$, giving:

$$M^* \frac{dT^*}{dM^*} + \left\{ 2 - k - NTU - \frac{M^*}{C_o^*} (NTU + NTU_\infty) \right\} \frac{dT^*}{dM^*} + \left\{ (k-1)(NTU + NTU_\infty) + NTU NTU_\infty \right\} \frac{T^*}{C_o^*} - \frac{NTU NTU_\infty}{C_o^*} T_\infty^* = 0$$

Similarly, for charging at constant mass flow:

$$M^* \frac{dT^*}{dM^*} + \left[2 + NTU + \frac{NTU + NTU_\infty}{C_o^*} M^* \right] \frac{dT^*}{dM^*} + [NTU NTU_\infty + NTU + NTU_\infty] \frac{T^*}{C_o^*} - \left(\frac{NTU + NTU_\infty}{C_o^*} \right) k T_i^* - \frac{NTU NTU_\infty}{C_o^*} T_\infty^* = 0$$

3. Adiabatic Charging and Blowdown



An energy balance on the gas in the receiver gives:

charging: $h, dM = d(Mu) = M du + u dM$

blowdown: $h dM = d(Mu) = M du + u dM$

Combining the energy balance and the equation of State:

charging: $(kT_i - T) dM = M dT$

blowdown: $(k-1) T dM = M dT$

Expressing in terms of nondimensional variables and separating:

charging: $\int_1^{T^*} \frac{dT^*}{(kT_i^* - T^*)} = \int_1^{M^*} \frac{dM^*}{M^*}$

blowdown: $\int_1^{T^*} \frac{dT^*}{T^*} = \int_1^{M^*} (k-1) \frac{dM^*}{M^*}$

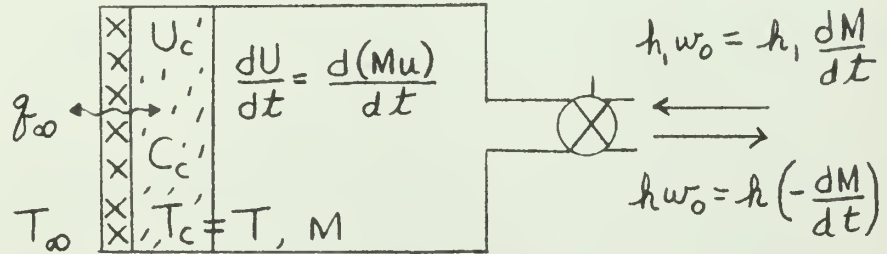
Integrating from the initial values to conditions at a later time:

Charging:
$$T^* = k T_i^* - \frac{k T_i^* - 1}{M^*} \quad (6)$$

Blowdown:
$$T^* = M^* (k-1) \quad (7)$$

4. Charging and Blowdown with Negligible Inside Resistance at Constant

Mass Flow



An energy balance on the gas and capacitance combined:

Charging:
$$h_1 \frac{dM}{dt} - q_\infty = C_c \frac{dT}{dt} + M \frac{du}{dt} + u \frac{dM}{dt}$$

Blowdown:
$$h \frac{dM}{dt} + q_\infty = C_c \frac{dT}{dt} + M \frac{du}{dt} + u \frac{dM}{dt}$$

A rate equation for the heat transfer resistance R_∞ , gives:

Charging:
$$q_\infty = \frac{T - T_\infty}{R_\infty}$$
 Blowdown:
$$q_\infty = \frac{T_\infty - T}{R_\infty}$$

Since, for charging: $w_o = dM/dt$ and for Blowdown: $w_o = -dM/dt$

Then, for charging:
$$\frac{dT}{dt} = \frac{dT}{dM} \frac{dM}{dt} = w_o \frac{dT}{dM}$$

for blowdown:
$$\frac{dT}{dt} = \frac{dT}{dM} \frac{dM}{dt} = -w_o \frac{dT}{dM}$$

Combining this relationship with the energy equation, rate equation, and the perfect gas equation of state, yields the following differential equation:

Charging:
$$\left(M + \frac{C_c}{C_v} \right) \frac{dT}{dM} - k T_i + T + \frac{T - T_\infty}{R_\infty C_v w_o} = 0$$

Blowdown:
$$\left(M + \frac{C_c}{C_v} \right) \frac{dT}{dM} + \frac{T_\infty - T}{R_\infty C_v w_o} - (k-1)T = 0$$

Expressing in terms of the dimensionless variables and separating:

$$\begin{aligned} \text{Charging: } & \int_1^{T^*} \frac{dT^*}{T^*(1+NTU_\infty) - kT_1^* - NTU_\infty T_\infty^*} + \int_1^{M^*} \frac{dM^*}{M^* + C_0^*} = 0 \\ \text{Blowdown: } & \int_1^{T^*} \frac{dT^*}{(k-1+NTU_\infty)T^* - T_\infty^* NTU_\infty} - \int_1^{M^*} \frac{dM^*}{M^* + C_0^*} = 0 \end{aligned}$$

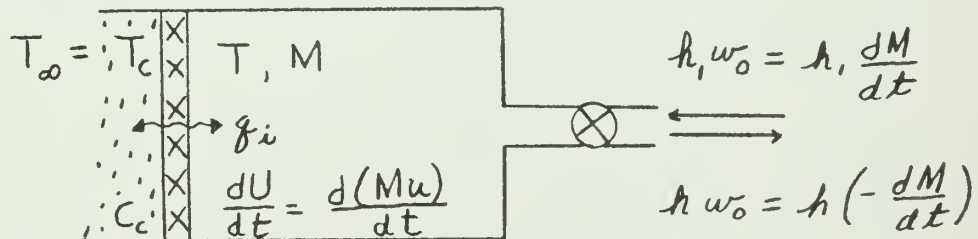
Integrating from the initial conditions to conditions at a later time:

$$\text{Charging: } T^* = \frac{(1+NTU_\infty - kT_1^* - NTU_\infty T_\infty^*) \left(\frac{C_0^* + 1}{C_0^* + M^*} \right)^{1+NTU_\infty} + kT_1^* + NTU_\infty T_\infty^*}{1+NTU_\infty} \quad (8)$$

$$\text{Blowdown: } T^* = \frac{(k-1+NTU_\infty - T_\infty^* NTU_\infty) \left(\frac{M^* + C_0^*}{1 + C_0^*} \right)^{k-1+NTU_\infty} + T_\infty^* NTU_\infty}{(k-1+NTU_\infty)} \quad (9)$$

5. Charging and Blowdown at Constant Mass Flow with Heat Transfer

To or From an Isothermal Source



An energy balance on the gas gives:

$$\text{Charging: } h_1 \frac{dM}{dt} = g_i + \frac{d(Mu)}{dt}$$

$$\text{Blowdown: } g_i + h \frac{dM}{dt} = M \frac{du}{dt} + u \frac{dM}{dt}$$

A rate equation for the heat transfer resistance R_i gives:

$$\text{Charging: } g_i = \frac{T - T_c}{R_i} \quad \text{Blowdown: } g_i = \frac{T_c - T}{R_i}$$

Since: for charging, $w_0 = dM/dt$ and for blowdown, $w_0 = -dM/dt$

Then:

$$\text{for charging: } \frac{dT}{dt} = \frac{dT}{dM} \cdot \frac{dM}{dt} = w_0 \frac{dT}{dM}$$

$$\text{for blowdown: } \frac{dT}{dt} = \frac{dT}{dM} \cdot \frac{dM}{dt} = -w_0 \frac{dT}{dM}$$

Combination of this relationship with the energy balance, rate equation, and perfect gas equation of state, gives:

$$\text{Charging: } M \frac{dT}{dM} + T - kT_i + \frac{T - T_c}{R_i c_v w_0} = 0$$

$$\text{Blowdown: } M \frac{dT}{dM} - \left[k-1 + \frac{1}{R_i c_v w_0} \right] T + \frac{T_c}{R_i c_v w_0} = 0$$

Expressing in terms of nondimensional variables and separating:

$$\text{Charging: } \int_1^{T^*} \frac{dT^*}{T^* (1+NTU) - kT_i^* - NTU T_c^*} = \int_1^{M^*} \left(-\frac{dM^*}{M^*} \right)$$

$$\text{Blowdown: } \int_1^{T^*} \frac{dT^*}{T_c^* NTU - (k-1+NTU) T^*} = - \int_1^{M^*} \frac{dM^*}{M^*}$$

Integrating from the initial values to conditions at a later time:

$$\text{Charging: } T^* = \frac{kT_i^* + NTU T_c^* - [kT_i^* - 1 - NTU + NTU T_c^*] M^{*(1+NTU)}}{1+NTU} \quad (10)$$

$$\text{Blowdown: } T^* = \frac{(k-1+NTU - T_c^* NTU) M^{*k+NTU} + T_c^* NTU}{k-1+NTU} \quad (11)$$

Or, integrating over the time interval Δt :

$$\text{Charging: } \int_{T^*}^{T^*+\Delta T^*} \frac{dT^*}{T^* (1+NTU) - kT_i^* - NTU T_c^*} = - \int_{M^*}^{M^*+\Delta M^*} \frac{dM^*}{M^*}$$

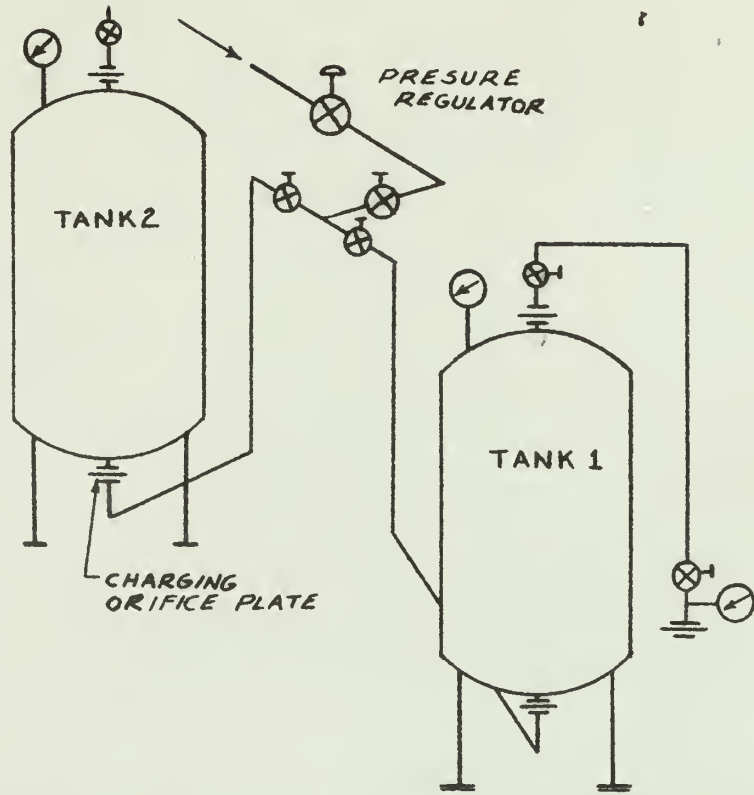
$$\text{Blowdown: } \int_{T^*}^{T^*+\Delta T^*} \frac{dT^*}{T_c^* NTU - (k-1+NTU) T^*} + \int_{M^*}^{M^*+\Delta M^*} \frac{dM^*}{M^*} = 0$$

Yields the stepwise equations:

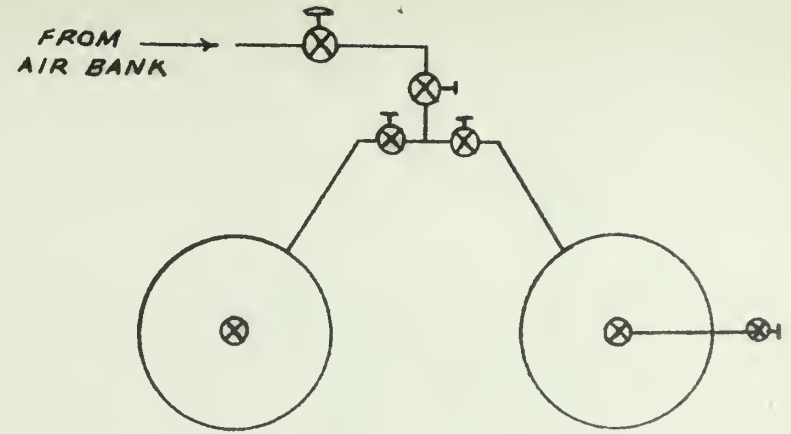
$$\text{Charging: } \Delta T^* = \left[\frac{kT_i^* + NTU T_c^*}{1+NTU} - T^* \right] \left[1 - \left(\frac{M^* + \Delta M^*}{M^*} \right)^{-(1+NTU)} \right] \quad (12)$$

$$\text{Blowdown: } \Delta T^* = \left[T^* - \frac{NTU}{k-1+NTU} T_c^* \right] \left[\left(\frac{M^* + \Delta M^*}{M^*} \right)^{k-1+NTU} - 1 \right] \quad (13)$$

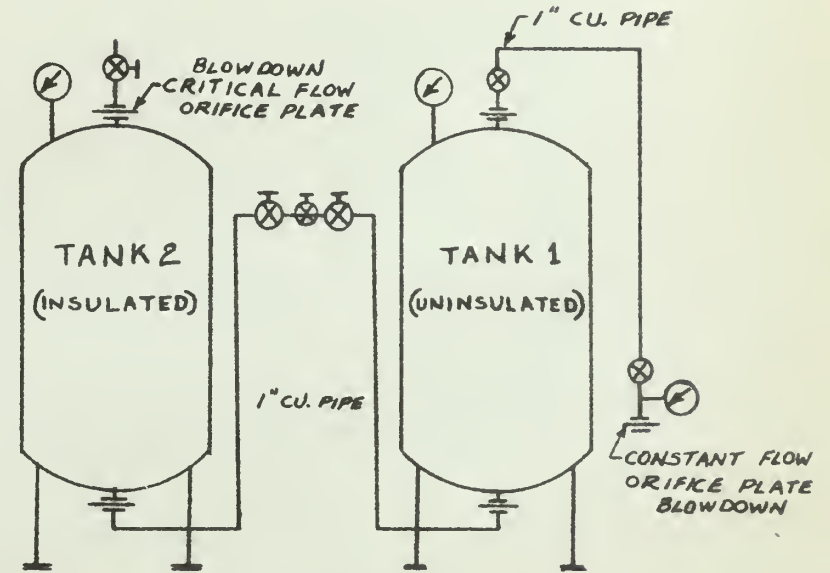
APPENDIX II
Figures 1 - 14



C. SCHEMATIC LAYOUT



a. TOP VIEW



b. PLAN VIEW

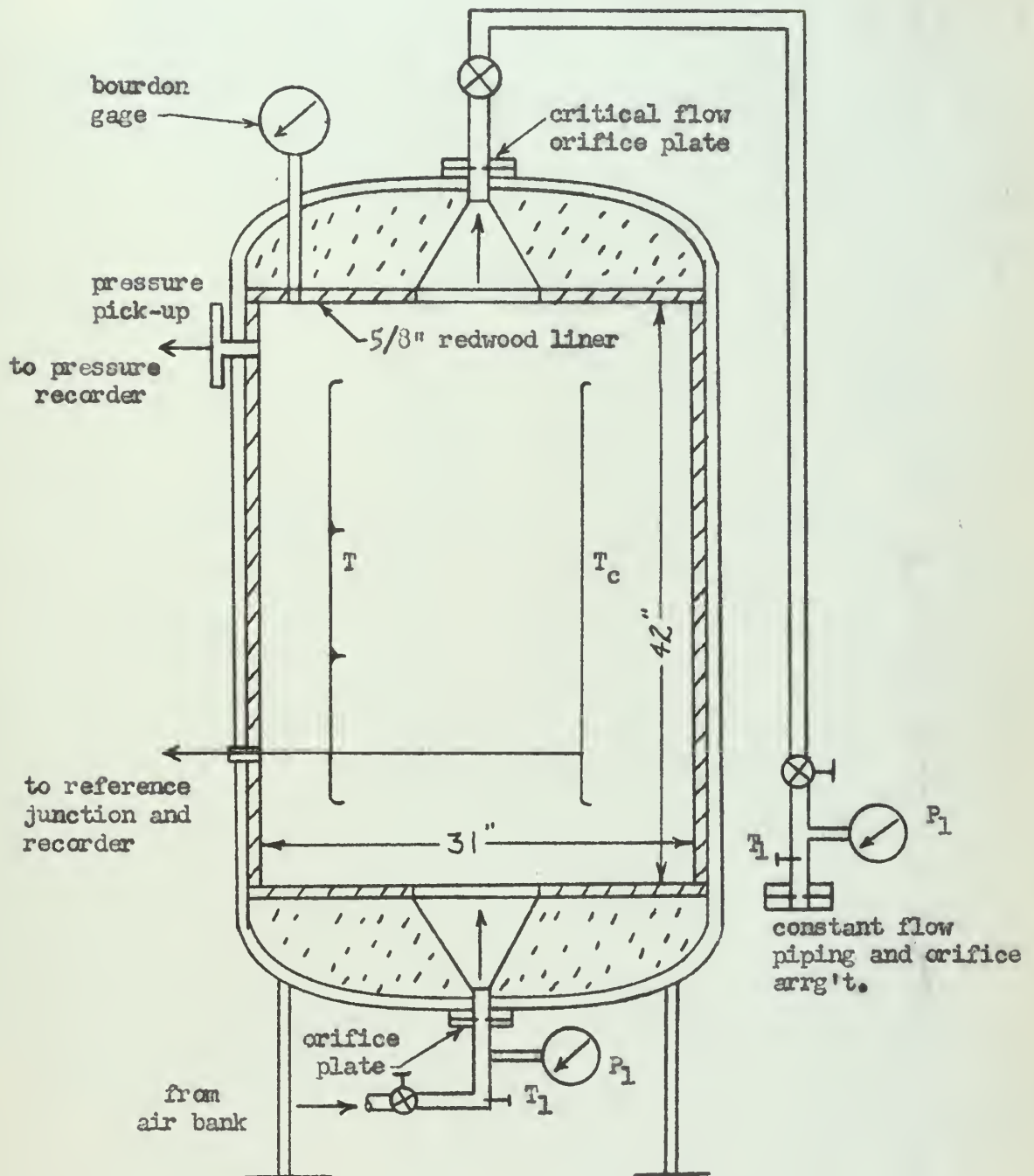
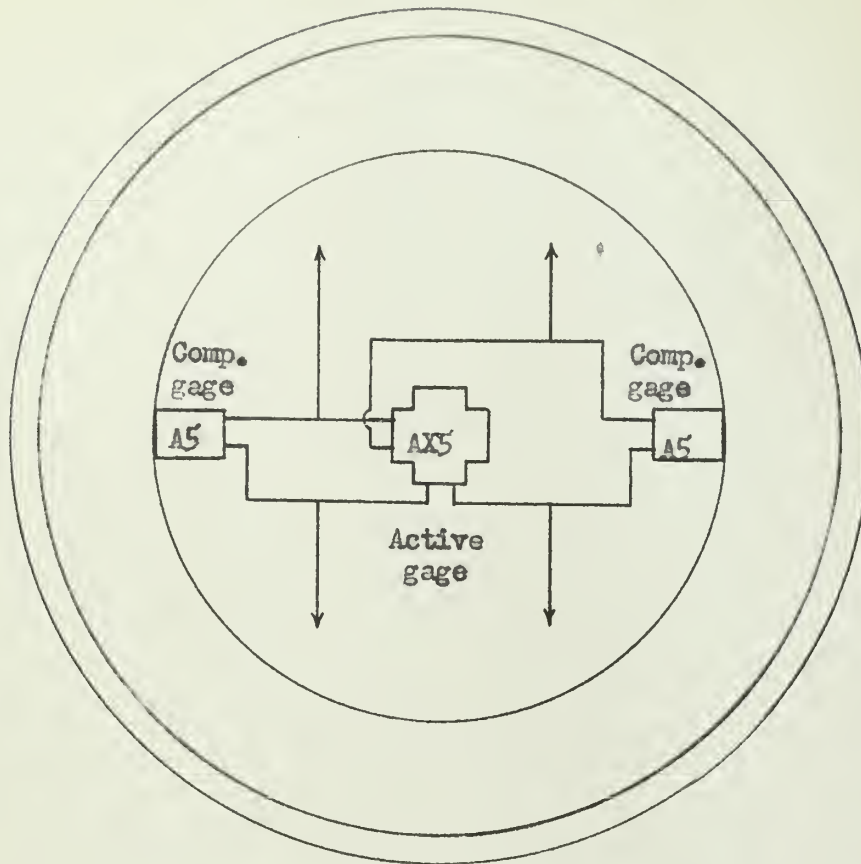


Diagram of the Insulated Tank

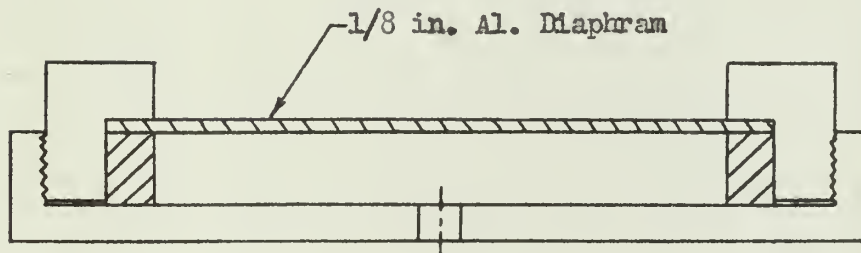
FIG. 2



Photograph of Test Apparatus
Fig. 3



a. Top View Showing Wiring Details



b. Cross Section View Showing Diaphragm

SR-4 STRAIN GAGE PRESSURE PICKUP

Fig. 4

T ADIABATIC SOL'N

CHARGING
UNINSULATED TANK
 $T_1^* = 0.990$ $T_c^* = 0.995$
 $C_o^* = 300$

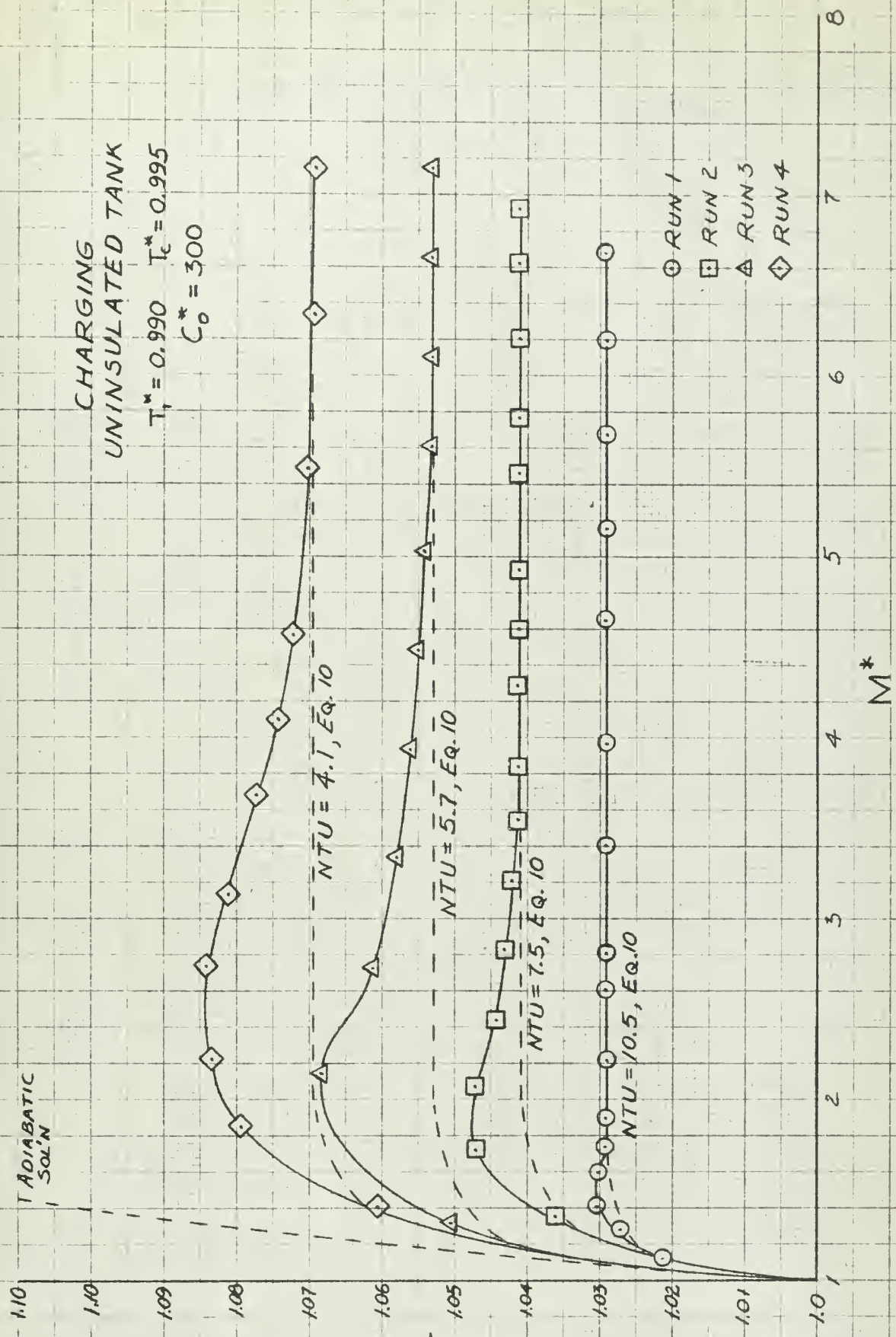


*
Fig. 5

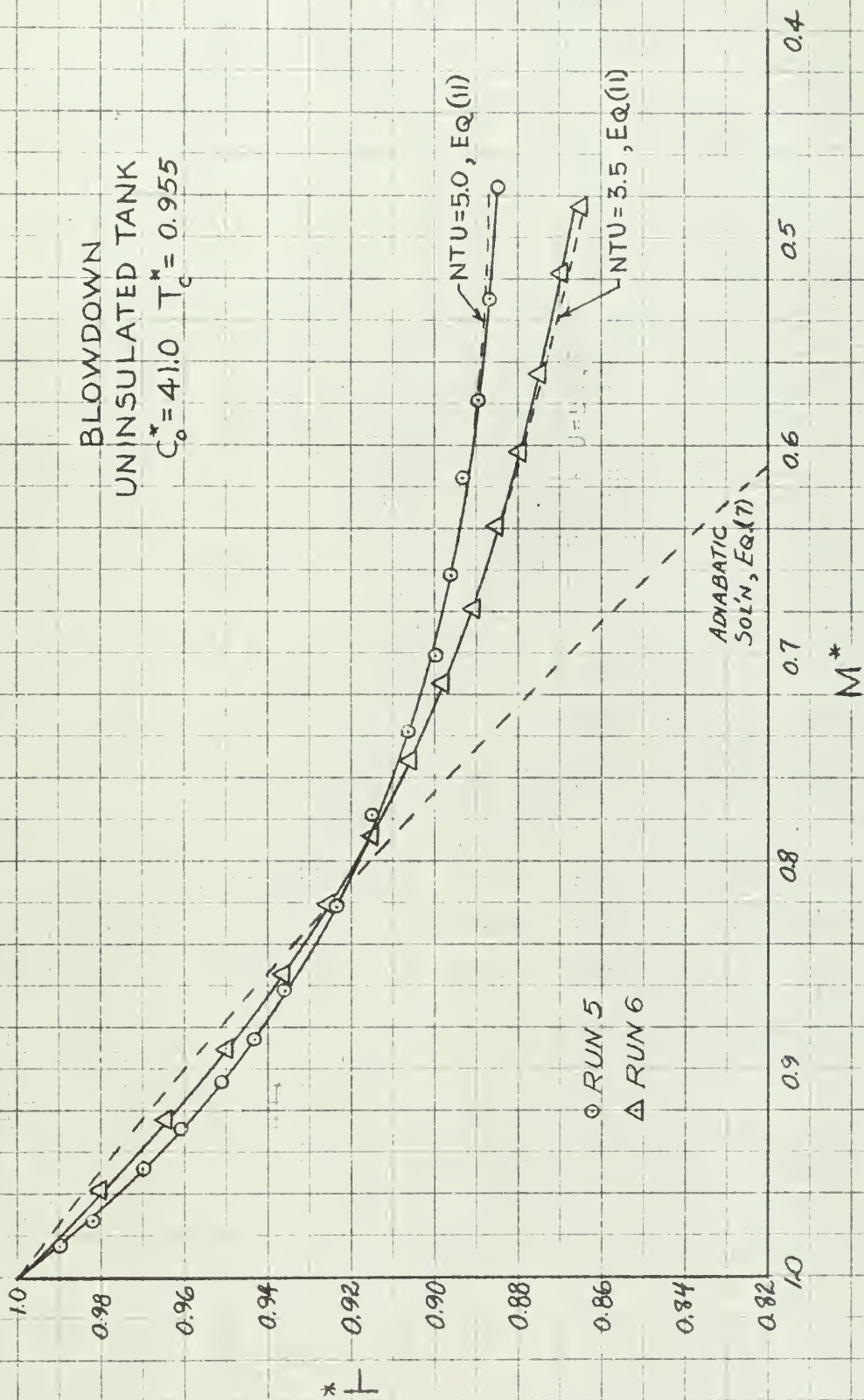


Fig. 6

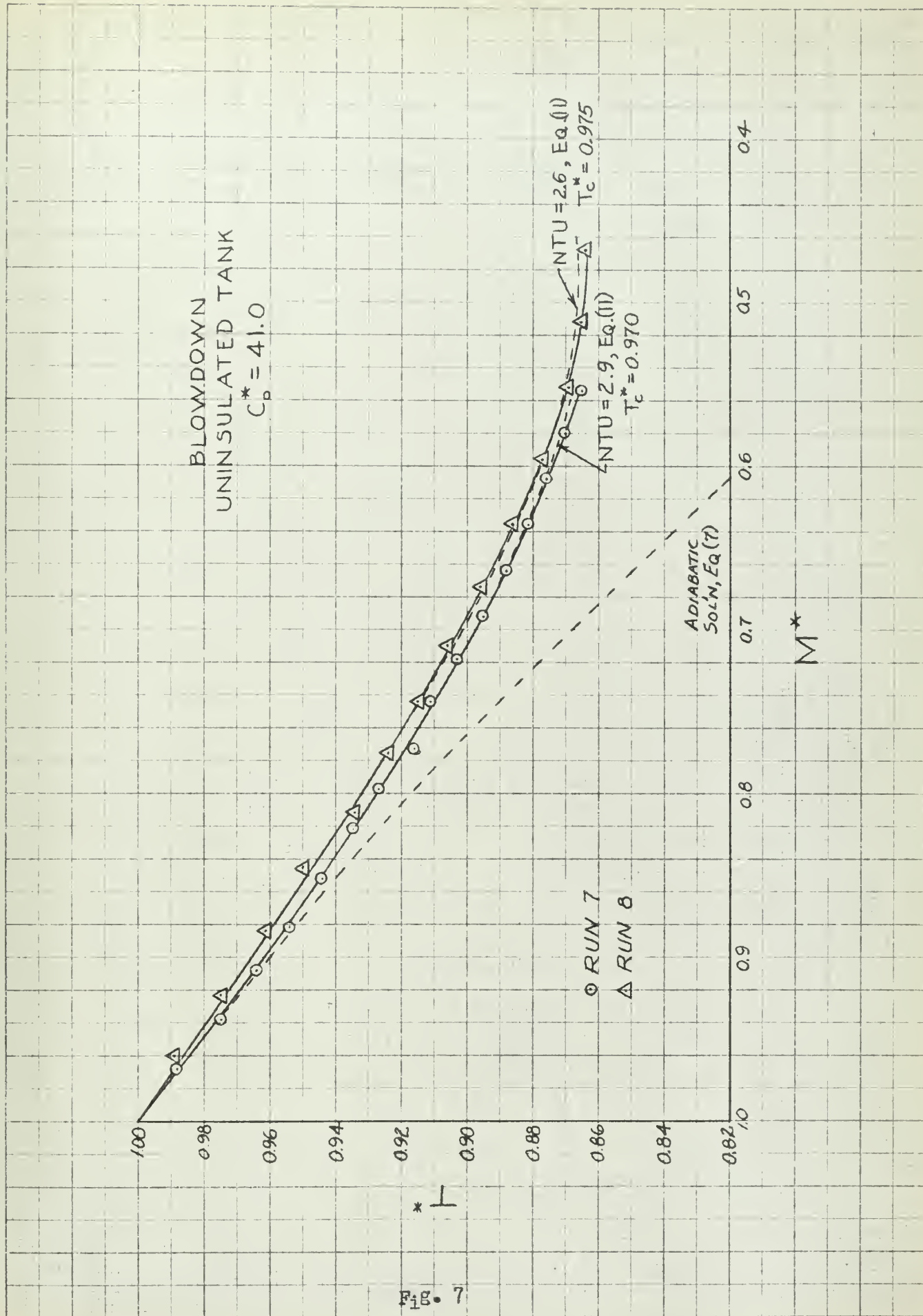


Fig. 7

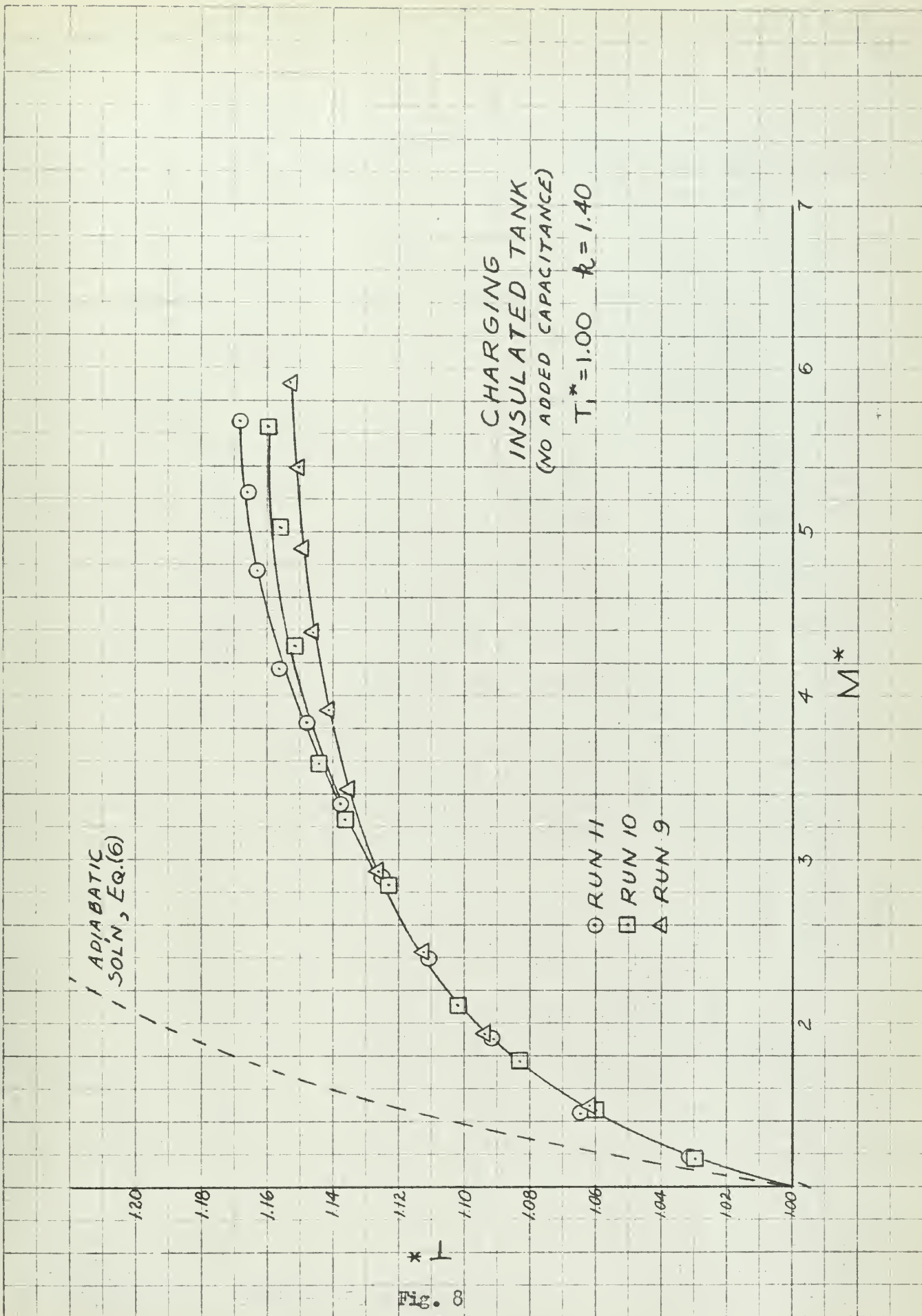
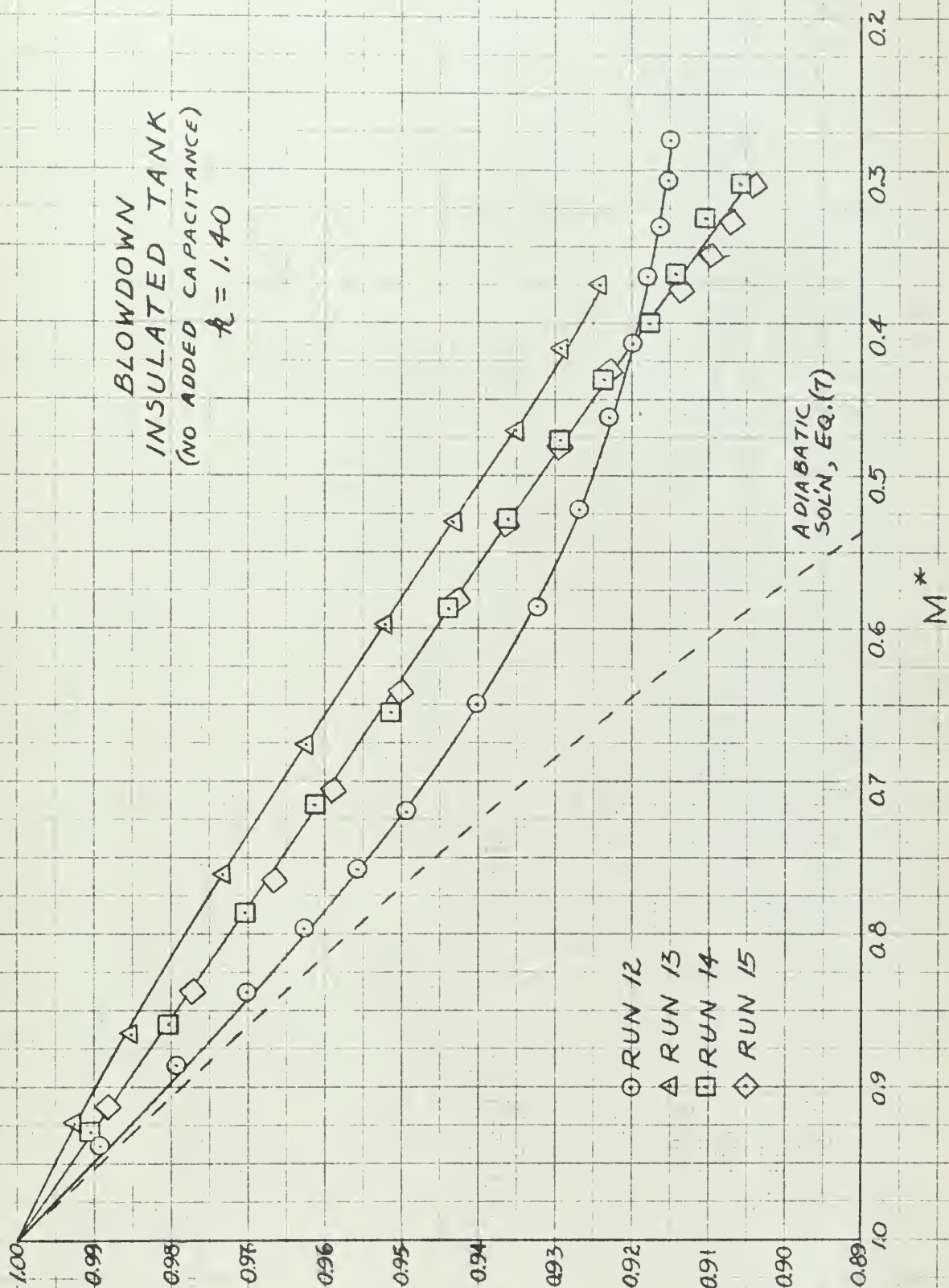


Fig. 8



* ⊥

Fig. 9

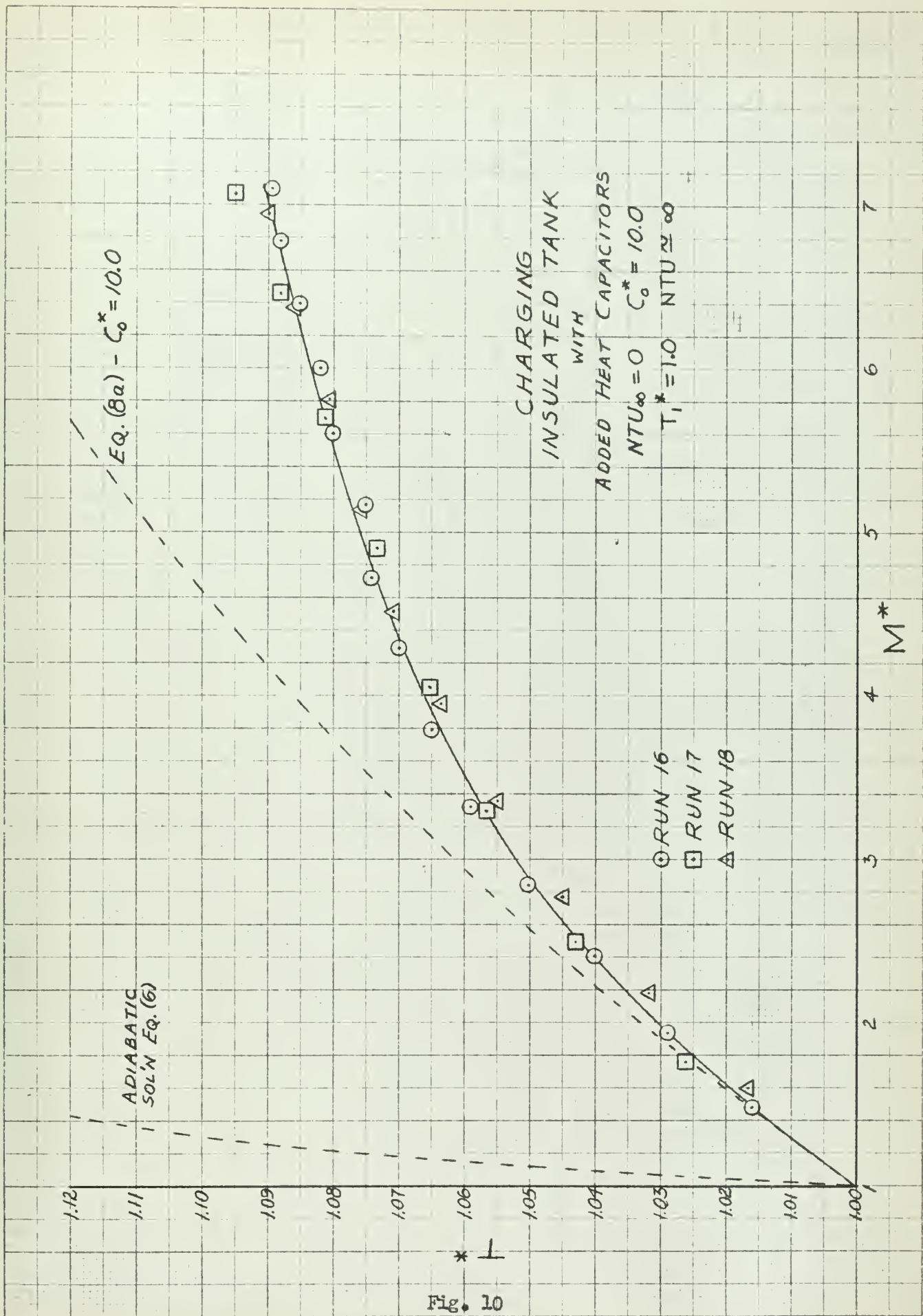


Fig. 10

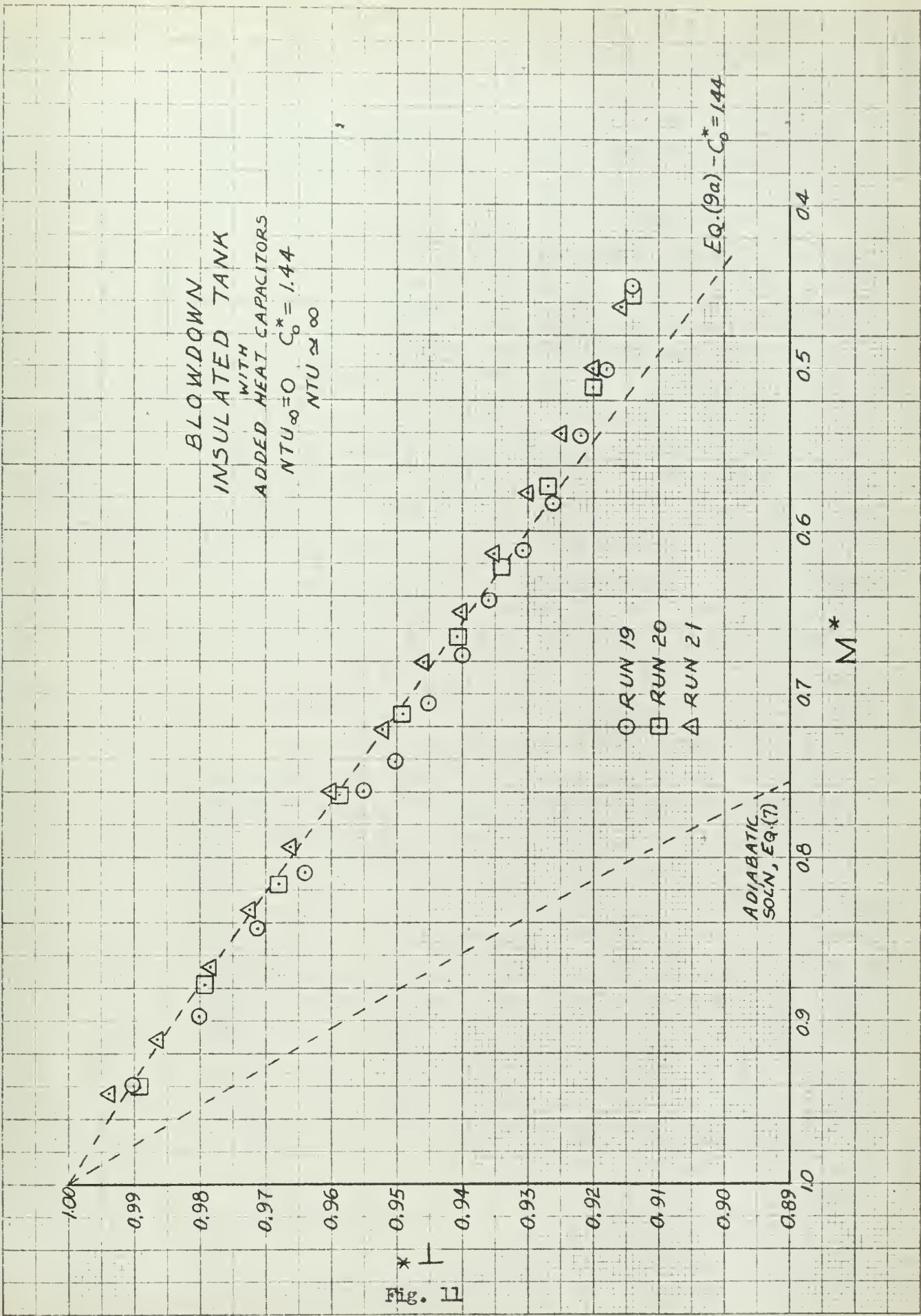


Fig. 11

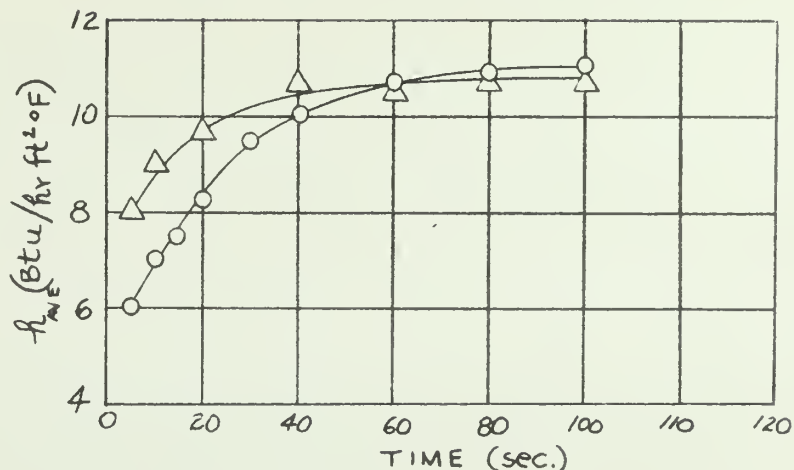
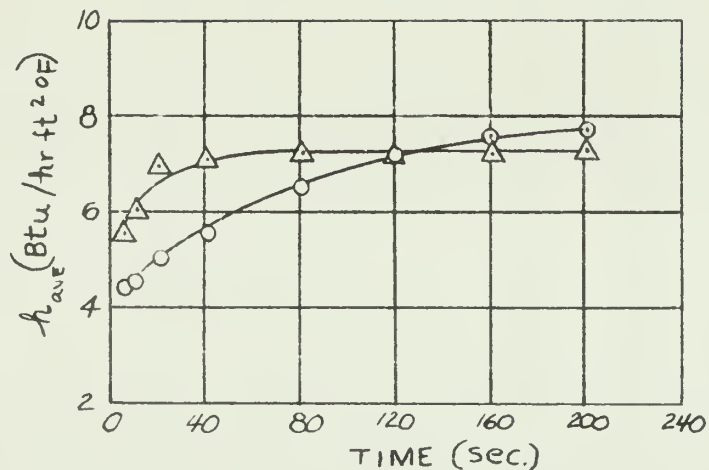
PREDICTED AVERAGE CONVECTIVE CONDUCTANCES
DURING
 CHARGING UNINSULATED TANK

○ - PREDICTED

△ - EXPERIMENTAL

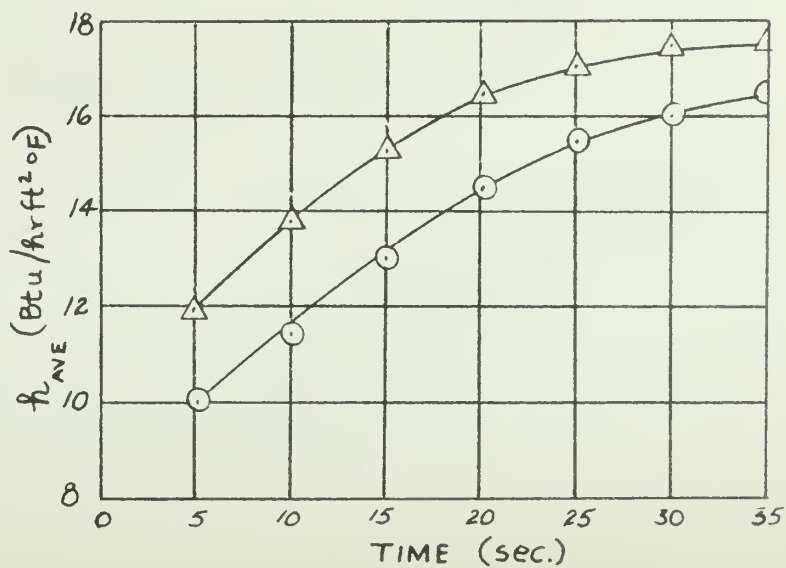
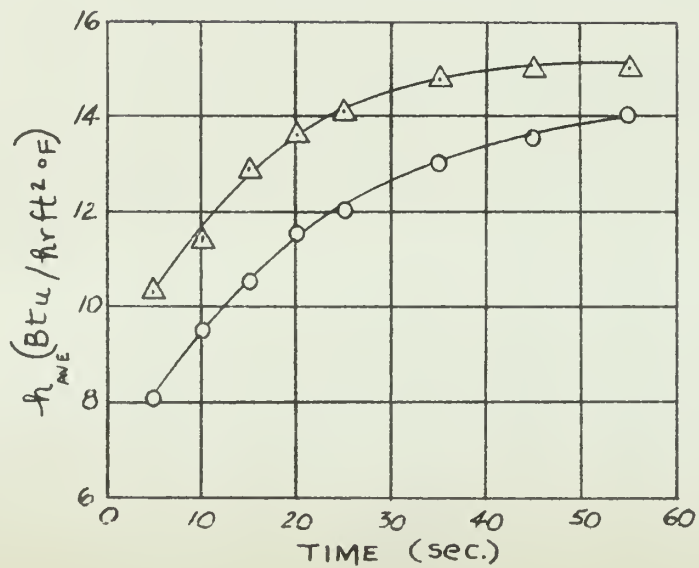
a. RUN 1 - 1/8" dia. ORIFICE

b. RUN 2 - 3/16" DIA. ORIFICE



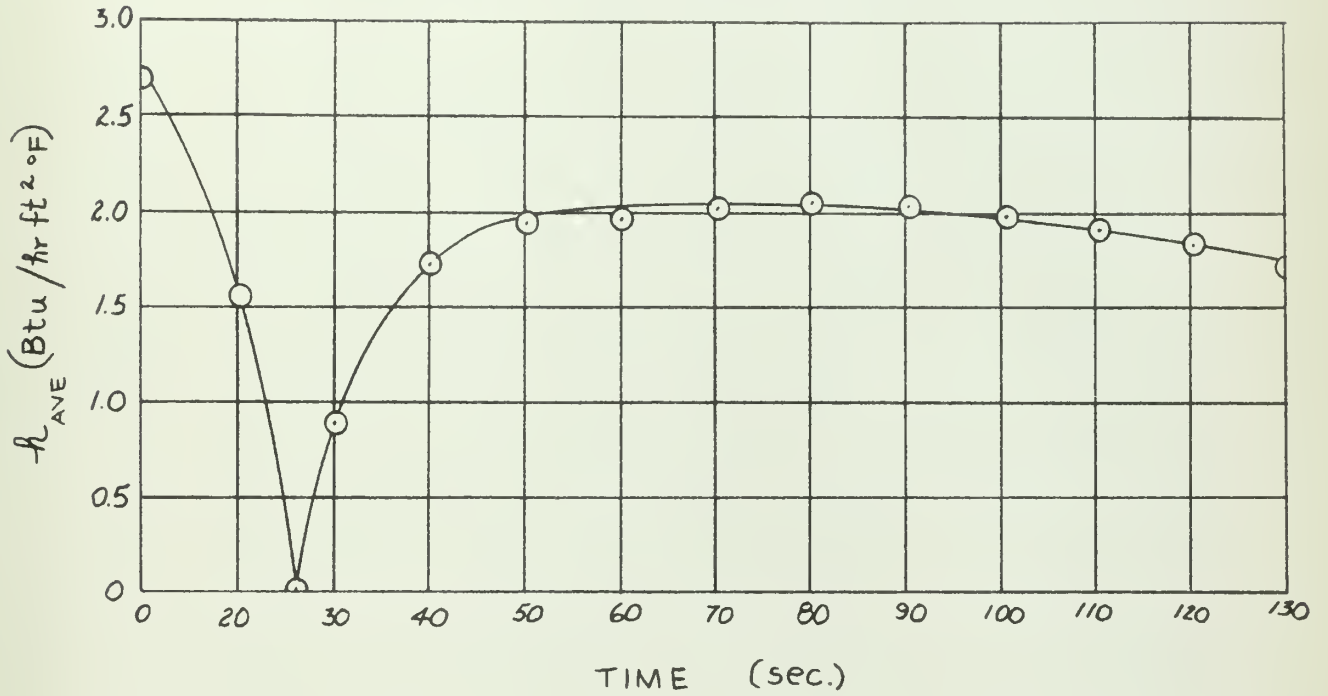
c. RUN 3 - 1/4" dia. ORIFICE

c. RUN 4 - 5/16" DIA. ORIFICE



Predicted Average Convective Conductances
 during
 Blowdown - Uninsulated Tank

a. Run 5, 3/16 in. dia. orifice



b. Run 6, 1/4 in. dia. orifice

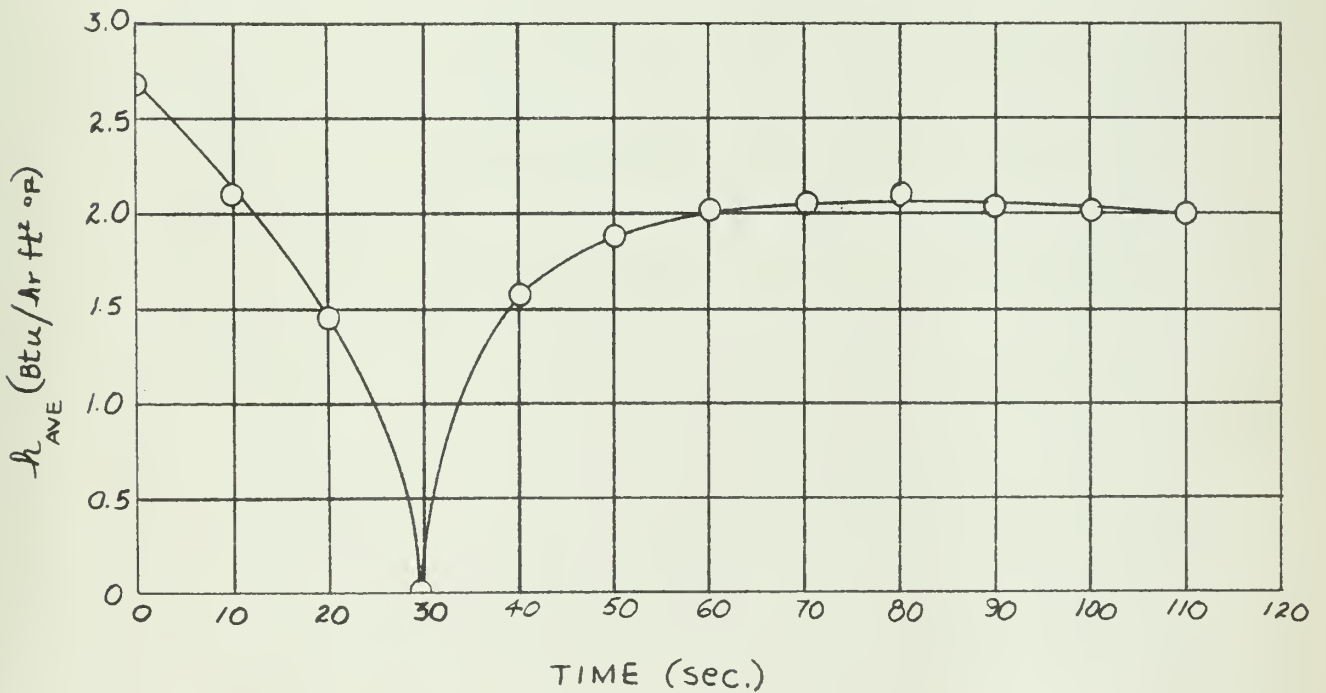
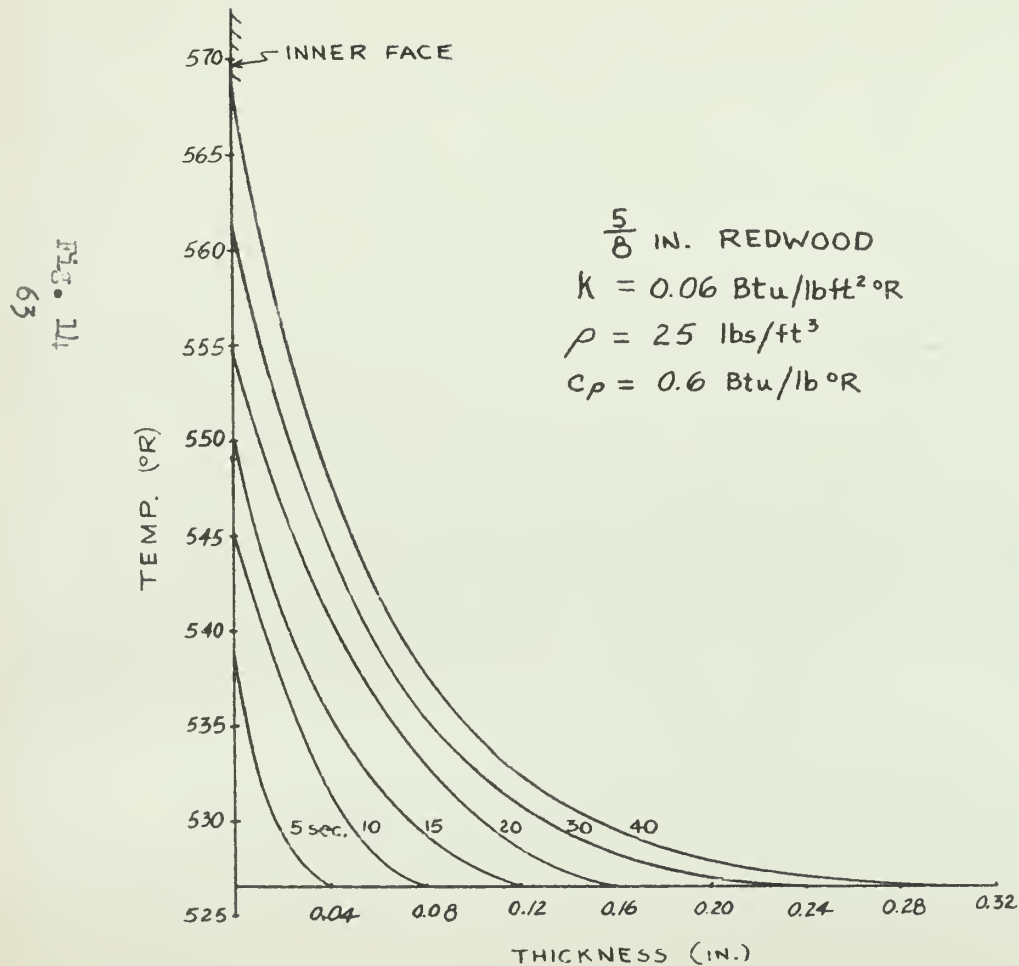


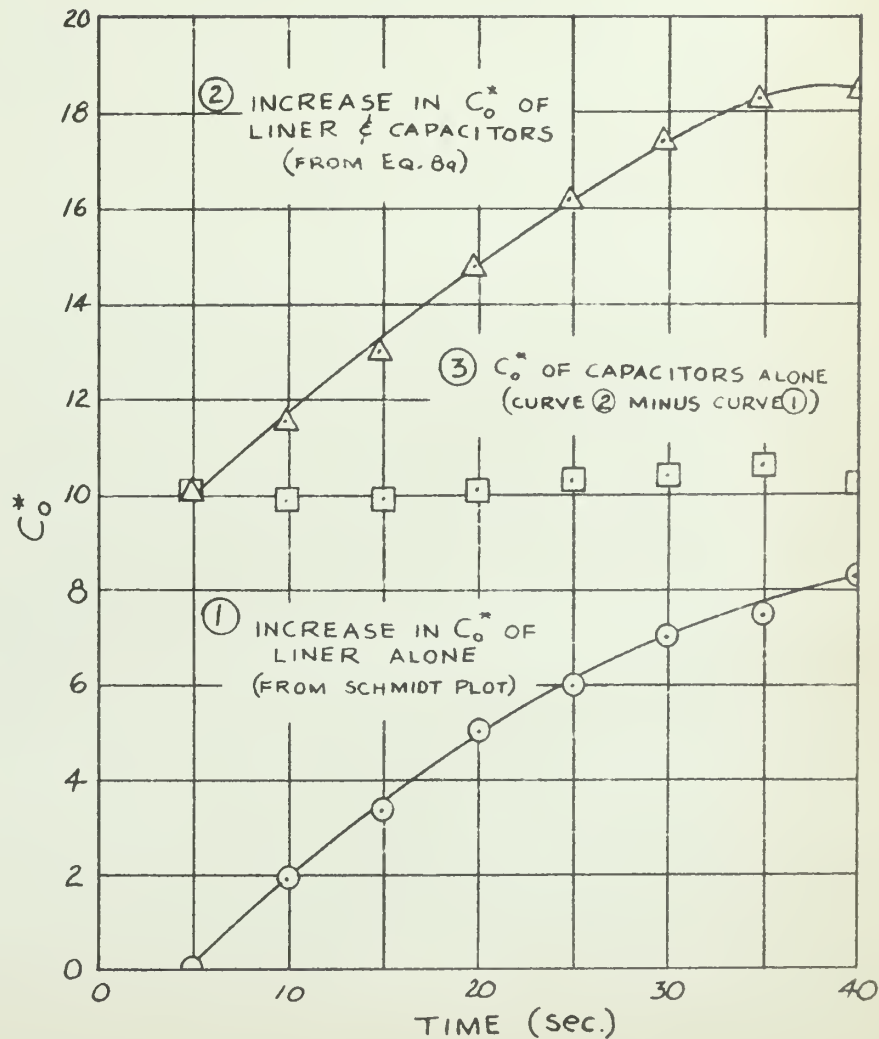
Fig. 13

EFFECT OF TANK LINER
ON C_o^* DURING CHARGING
RUN 17

a. SCHMIDT PLOT SOLUTION FOR
TEMPERATURE DISTRIBUTION
IN REDWOOD LINER



b. CHANGE OF C_o^* WITH TIME



APPENDIX III

Solution of the General Differential Equation for
Constant Mass Flow Blowdown by Analog Computer Methods

APPENDIX III

Solution of the General Differential Equation for Constant Mass Flow

Blowdown by Analog Computer Methods

1. Derivation of the Machine Equation

Equation (2a) (Appendix I) may be rearranged in the case of

$NTU_{\infty} = 0$ as follows:

$$\frac{d^2 T^*}{dM^*} + \frac{\alpha}{M^*} \frac{dT^*}{dM^*} - \gamma \frac{dT^*}{dM^*} + \delta \frac{T^*}{M^*} = 0 \quad (2b)$$

The constants α, γ, δ are defined in terms of the system parameters as follows:

$$\alpha = 2 - k - NTU \quad (25)$$

$$\gamma = \frac{NTU}{C_o^*} \quad (26)$$

$$\delta = (k-1) \frac{NTU}{C_o^*} \quad (27)$$

Equation (2b) is readily adaptable for solution by analog computer.

Adopting the standard nomenclature of Korn [11], the variables of equation (2b) may be expressed in terms of computer voltages and functions as follows:

$$\bar{T} = a_T T^* \quad (28)$$

$$\bar{M} = a_M M^* \quad (29)$$

$$\frac{d}{dM^*} = a_t \frac{d}{dt} = a_t p \quad (30)$$

In the above transfer functions, a_T and a_M are scale factors relating the machine voltages \bar{T} and \bar{M} to the variables T^* and M^* and a_t is the time-scale factor relating differentiation with respect to the variable M^* to the standard operator p denoting differentiation with respect to machine time t .

Substituting the transfer functions in equation (2b) results in the following machine equation for the general case of constant mass flow blowdown:

$$a_T p^2 \bar{T} = -\frac{a_M}{\bar{M}} \left(\alpha p \bar{T} + \frac{\delta \bar{T}}{a_t} \right) + \gamma p \bar{T} \quad (2c)$$

The initial conditions to be employed in the integration of equation (2b) are given by Reynolds [2] as follows:

$$\text{At } M_o^* = 1: \quad T_o^* = 1 \quad \text{and} \quad \left. \frac{dT^*}{dM} \right|_o = k - 1 + NTU - NTU T_c^* \quad (31)$$

2. Block Diagram for Analog Computer Setup

Machine equation (2c) combined with the initial conditions is represented in block diagram form for solution by d-c analog computer as follows:

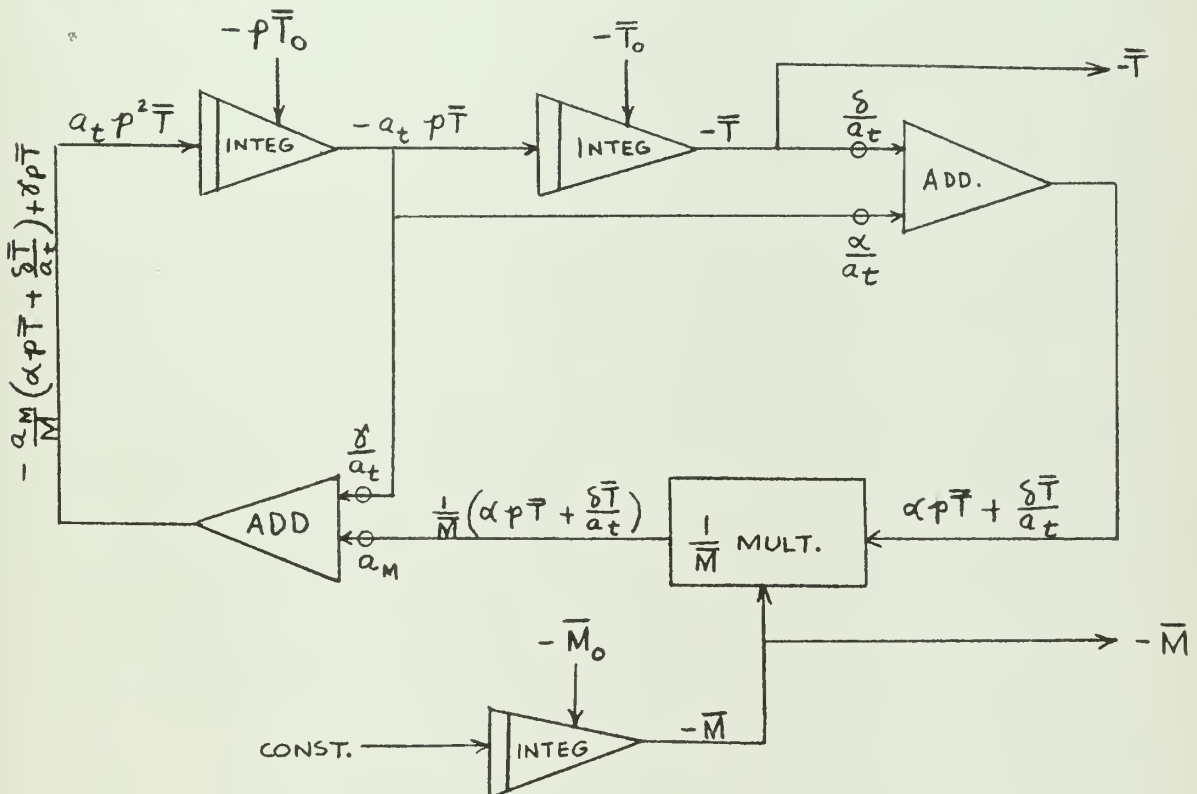


Figure 15

Analog Computer Setup for Solution of General Equation for Constant Flow Blowdown

3. Evaluation of Analog Computer Solutions

The analog computer block diagram of Fig. 15, suitably time and magnitude scaled, was set up on a Boeing Model 7079 Analog Computer with the output to a Reeve servo plotting board. It was originally planned to compare the computer blowdown solutions with those obtained from the simplified blowdown equations (Chapter 5) best fitting the experimental data. The solutions, although capable of qualitatively reproducing the general solutions shown in Fig. 1 of reference [2], were not sensitive enough to changes in the system parameters to prove reliable.

Solutions for both the case of infinite capacitance and the case of negligible internal resistance were attempted with the computer. In the infinite capacitance case in which δ and ξ both approach zero (equations 26 and 27), the computer plot showed a barely discernable change over a range of several integer values of NTU in equation (25). The same held true for the case of negligible internal resistance. Here, since C_0^* has a finite value, changes in NTU affect δ and ξ as well as α . Once again, however, quite large changes in the value of NTU had little effect on the displacement of the computer solution.

This lack of sensitivity is in part due to the fact that the experimental data lies, in all cases, in a narrow range of T^* and M^* close to the origin of the graphical plot. In this range, Fig. 1 of reference [2] shows that there is little change in the trend of the general solution despite large differences in the magnitude of the system parameters. Attempts to enlarge the scale resulted in an unreliable performance of the plotting equipment. This program, however, could be of value where lower values of T^* and M^* were of interest, since in this region the general solution diverges sufficiently to reflect smaller changes in NTU.

APPENDIX IV
Experimental Data

Table 11

Charging Run Data- Uninsulated TankRun 1

Orifice: 1/3 in. dia. $w_0 = 100 \text{ lb/hr}$
 $C_0^* = 300$ $T_1^* = 0.990$ $T_c^* = 0.995$

<u>t</u> (sec)	<u>T</u> (°R)	<u>P</u> (psia)	<u>T*</u>	<u>P*</u>	<u>M*</u>
0	537	14.3	1.000	1.00	1.00
5	543	17.2	1.021	1.16	1.14
10	551	19.5	1.027	1.32	1.29
20	553	24.5	1.029	1.65	1.60
30	552	28.9	1.029	1.95	1.90
40	552	33.7	1.029	2.23	2.22
50	552	38.5	1.029	2.59	2.60
60	552	42.9	1.029	2.90	2.82
80	552	51.8	1.029	3.50	3.40
100	552	60.7	1.029	4.10	3.93
120	552	69.6	1.029	4.70	4.66
140	552	78.5	1.029	5.30	5.15
160	552	86.5	1.029	5.85	5.63
180	552	94.5	1.029	6.33	6.20
200	552	101.8	1.029	6.87	6.68

Run 2

Orifice: 3/16 in. dia. $w_0 = 300 \text{ lb/hr}$
 $C_0^* = 300$ $T_1^* = 0.990$ $T_c^* = 0.995$

<u>t</u> (sec)	<u>T</u> (°R)	<u>P</u> (psia)	<u>T*</u>	<u>P*</u>	<u>M*</u>
0	537	14.3	1.000	1.00	1.00
10	562	26.7	1.047	1.30	1.72
20	561	37.9	1.044	2.56	2.45
30	560	49.6	1.042	3.35	3.21
40	559	60.7	1.041	4.10	3.93
50	559	71.0	1.041	4.80	4.61
60	559	80.6	1.041	5.45	5.45
70	559	88.8	1.041	6.00	5.76
80	559	95.7	1.041	6.47	6.20
85	559	99.2	1.041	6.70	6.43
90	559	102.0	1.041	6.90	6.62
95	559	104.3	1.041	7.03	6.80
100	559	106.3	1.041	7.22	6.92

Table 11
(continued)

Run 3

Orifice: 1/4 in. dia. $w_0 = 711 \text{ lb/hr}$

$C_o^* = 300$ $T_1^* = 0.990$ $T_c^* = 0.995$

<u>t</u> (sec)	<u>T</u> (°R)	<u>P</u> (psia)	<u>T</u> [*]	<u>P</u> [*]	<u>M</u> [*]
0	538	14.8	1.000	1.00	1.00
5	566	20.4	1.050	1.33	1.32
10	575	34.1	1.063	2.30	2.15
15	572	42.3	1.061	2.89	2.72
20	569	52.3	1.059	3.53	3.34
25	563	61.4	1.056	4.15	3.93
30	563	70.2	1.055	4.74	4.49
35	567	75.5	1.054	5.30	5.03
40	567	87.4	1.053	5.90	5.60
45	567	95.2	1.053	6.44	6.10
50	567	103.4	1.053	6.93	6.64
55	567	111.0	1.053	7.50	7.13

Run 4

Orifice: 5/16 in. dia. $w_0 = 1140 \text{ lb/hr}$

$C_o^* = 300$ $T_1^* = 0.990$ $T_c^* = 0.995$

<u>t</u> (sec)	<u>T</u> (°R)	<u>P</u> (psia)	<u>T</u> [*]	<u>P</u> [*]	<u>M</u> [*]
0	532	14.8	1.000	1.00	1.00
2.5	564	22.2	1.060	1.50	1.41
5.0	574	29.6	1.079	2.00	1.35
7.5	576	35.8	1.033	2.42	2.13
10.0	577	44.2	1.034	2.93	2.75
12.5	575	50.3	1.031	3.40	3.14
15.0	573	53.4	1.077	3.94	3.63
17.5	572	65.2	1.074	4.40	4.10
20.0	571	72.5	1.072	4.90	4.57
25.0	569	85.8	1.070	5.30	5.47
30.0	568	99.2	1.069	6.70	6.33
35.0	568	111.3	1.069	7.55	7.14

Table 12

Blowdown Run Data - Uninsulated TankRun 5

Orifice: 3/16 in. dia.

 $w_0 = 105 \text{ lb/hr}$ $C_0^* = 41.0$ $T_c^* = 0.955$

<u>t</u> (sec)	<u>T</u> (°R)	<u>P</u> (psia)	<u>T</u> [*]	<u>P</u> [*]	<u>M</u> [*]
0	560	114.8	1.000	1.000	1.000
10	550	109.5	.982	.955	.973
20	543	105.5	.970	.920	.943
40	533	98.6	.951	.860	.906
60	524	92.5	.936	.806	.862
80	517	87.3	.924	.760	.823
100	514	81.9	.916	.714	.778
120	503	77.0	.903	.670	.733
140	503	72.3	.899	.630	.702
160	502	68.2	.896	.594	.663
180	500	63.2	.893	.550	.617
200	493	58.8	.889	.513	.573
220	496	54.0	.886	.470	.530
240	494	49.2	.884	.420	.475

Run 6

Orifice: 1/4 in. dia.

 $w_0 = 166 \text{ lb/hr}$ $C_0^* = 41.0$ $T_c^* = 0.955$

<u>t</u> (sec)	<u>T</u> (°R)	<u>P</u> (psia)	<u>T</u> [*]	<u>P</u> [*]	<u>M</u> [*]
0	560	113.8	1.000	1.000	1.000
5	553	110.2	.983	.970	.982
10	543	107.0	.980	.940	.950
15	543	104.2	.970	.916	.945
20	539	101.0	.964	.930	.924
30	532	96.1	.950	.845	.890
40	526	91.0	.936	.800	.855
50	513	86.5	.926	.760	.821
60	513	81.8	.915	.720	.788
80	503	73.0	.893	.642	.714
100	496	63.3	.885	.566	.639
120	490	56.4	.875	.495	.566
140	485	47.7	.865	.420	.500

Table 12
(continued)

Run 7

Orifice: 5/16 in. dia.

$w_0 = 257$ lb/hr

$C_0^* = 41.0$

$T_c^* = 0.970$

<u>t</u> (sec)	<u>T</u> (°R)	<u>P</u> (psia)	<u>T*</u>	<u>P*</u>	<u>M*</u>
0	564	114.8	1.000	1.000	1.000
5	554	109.0	.983	.950	.966
10	547	104.5	.970	.910	.940
15	540	100.2	.953	.874	.913
20	534	96.4	.943	.840	.886
25	530	92.0	.940	.803	.854
30	525	88.4	.931	.770	.826
35	520	84.8	.923	.740	.802
40	516	81.2	.915	.708	.774
45	512	77.5	.907	.676	.746
50	507	74.2	.900	.646	.717
55	504	70.6	.893	.616	.690
60	500	67.2	.887	.586	.660
65	497	64.0	.881	.558	.633
70	494	60.6	.876	.528	.603

Run 8

Orifice: 3/8 in. dia.

$w_0 = 375$ lb/hr

$C_0^* = 41.0$

$T_c^* = 0.975$

<u>t</u> (sec)	<u>T</u> (°R)	<u>P</u> (psia)	<u>T*</u>	<u>P*</u>	<u>M*</u>
0	548	116.1	1.000	1.000	1.000
5	542	110.3	.989	.950	.961
10	534	104.4	.975	.900	.923
15	527	98.7	.961	.850	.885
20	521	93.2	.950	.803	.845
25	513	88.2	.935	.760	.813
30	507	83.3	.924	.717	.776
40	497	74.3	.906	.644	.710
60	477	57.3	.869	.480	.553
65	475	51.3	.865	.442	.511
70	474	46.3	.864	.404	.468

Table 13

Charging Run Data- Insulated TankRun 9Orifice: 5/16 in. dia. $w_0 = 1130$ lb/hr

$T_1^* = 0.998$

<u>t</u> (sec)	<u>T</u> (°R)	<u>P</u> (psia)	<u>T*</u>	<u>P*</u>	<u>M*</u>
0	532	14.3	1.000	1.00	1.00
2	565	23.7	1.061	1.60	1.50
4	532	32.1	1.094	2.17	1.93
6	592	40.4	1.113	2.73	2.45
8	593	43.3	1.126	3.30	2.93
10	604	57.7	1.135	3.90	3.43
12	607	66.0	1.141	4.46	3.91
14	610	74.5	1.146	5.03	4.39
16	612	83.1	1.149	5.62	4.90
18	613	91.3	1.151	6.20	5.39
20	614	101.0	1.153	6.80	5.90

Run 10Orifice: 3/8 in. dia. $w_0 = 1320$ lb/hr

$T_1^* = 0.993$

<u>t</u> (sec)	<u>T</u> (°R)	<u>P</u> (psia)	<u>T*</u>	<u>P*</u>	<u>M*</u>
0	523	14.3	1.000	1.00	1.00
1	545	18.1	1.030	1.22	1.13
2	562	23.1	1.060	1.56	1.47
3	573	28.5	1.083	1.93	1.73
4	583	34.3	1.101	2.32	2.11
5	590	40.7	1.114	2.75	2.47
6	594	47.4	1.123	3.20	2.85
8	601	54.5	1.136	3.63	3.24
10	605	60.7	1.144	4.10	3.59
12	608	73.3	1.151	4.95	4.30
14	611	85.3	1.157	5.80	5.02
16	612	96.6	1.159	6.53	5.64

Table 13
(continued)

Run 11

Orifice: 7/16 in. dia. $w_0 = 1960$ lb/hr

$T_1^* = 1.00$

<u>t</u> (sec)	<u>T</u> (°R)	<u>P</u> (psia)	<u>T*</u>	<u>P*</u>	<u>M*</u>
0	530	14.8	1.000	1.00	1.00
1	534	17.3	1.032	1.20	1.16
2	539	22.3	1.065	1.54	1.45
3	561	30.3	1.092	2.03	1.70
4	576	35.5	1.112	2.67	2.40
5	533	42.6	1.126	3.24	2.83
6	505	49.4	1.138	3.30	3.34
7	602	54.3	1.143	4.40	3.84
8	603	61.6	1.156	4.30	4.16
9	612	70.4	1.163	5.53	4.76
10	615	77.6	1.166	6.10	5.24
11	617	93.9	1.168	6.63	5.67

Table 14

Blowdown Run Data- Insulated Tank

Run 12

Orifice: 1/4 in. dia. $w_0 = 395$ lb/hr

<u>t</u> (sec)	<u>T</u> (°R)	<u>P</u> (psia)	<u>T*</u>	<u>P*</u>	<u>M*</u>
0	599	115.7	1.000	1.000	1.000
10	574	95.0	.953	.343	.335
20	555	85.1	.925	.736	.796
30	533	74.6	.899	.616	.719
40	527	66.0	.880	.571	.643
50	513	58.4	.864	.55	.535
60	512	51.4	.853	.445	.522
70	507	45.1	.845	.390	.462
80	502	39.3	.839	.345	.412
90	500	35.5	.835	.307	.363
100	493	32.4	.832	.280	.337
110	497	29.4	.830	.254	.306
120	496	26.3	.829	.232	.280

Table 11
(continued)

Run 13

Orifice: 3/3 in. dia.

$w_0 = 341 \text{ lb/hr}$

<u>t</u> (sec)	<u>T</u> (°R)	<u>P</u> (psia)	<u>T*</u>	<u>P*</u>	<u>M*</u>
0	535	111.3	1.000	1.000	1.000
2.5	576	101.4	.935	.910	.924
5	567	90.1	.947	.720	.761
10	554	75.0	.930	.700	.705
15	541	69.5	.925	.625	.676
20	528	60.1	.904	.540	.598
25	518	52.3	.886	.470	.530
30	508	45.5	.870	.409	.470
35	502	39.7	.858	.357	.416
40	496	35.2	.848	.316	.375

Run 14

Orifice: 7/16 in. dia.

$w_0 = 360 \text{ lb/hr}$

<u>t</u> (sec)	<u>T</u> (°R)	<u>P</u> (psia)	<u>T*</u>	<u>P*</u>	<u>M*</u>
0	615	93.3	1.000	1.000	1.000
2.5	602	87.8	.976	.838	.914
5	587	78.6	.954	.796	.838
7.5	574	70.6	.933	.715	.766
10	564	64.0	.917	.647	.707
12.5	554	57.2	.900	.578	.642
15	544	50.7	.885	.513	.580
17.5	536	45.7	.872	.463	.531
20	528	41.0	.859	.415	.483
22.5	521	37.1	.846	.375	.443
25	514	34.0	.835	.344	.412
27.5	508	31.1	.826	.315	.381
30	503	29.0	.818	.293	.358
32.5	500	27.0	.813	.273	.336
35	497	24.8	.809	.251	.311

Table 14
(continued)

Run 15

Orifice: 1/2 in. dia.

$w_0 = 1100$ lb/hr

<u>t</u> (sec)	<u>T</u> (°R)	<u>P</u> (psia)	<u>T*</u>	<u>P*</u>	<u>M*</u>
0	616	114.3	1.000	1.000	1.000
2	604	104.4	.930	.910	.923
4	592	94.7	.960	.825	.858
6	581	85.0	.942	.740	.756
8	569	75.7	.922	.660	.714
10	556	67.7	.902	.590	.654
12	547	59.7	.837	.520	.586
14	537	51.7	.872	.460	.527
16	530	47.1	.858	.410	.477
18	522	42.5	.846	.370	.437
20	515	38.3	.835	.334	.400
22	510	34.8	.828	.303	.367
24	505	31.3	.820	.273	.333
26	499	28.7	.810	.250	.309

Table 15

Charging Run Data- Insulated Tank
with Added Capacitors

Run 16

Orifice: 3/16 in. dia.

$w_0 = 407$ lb/hr

$C_0^* = 10.0$

$T_1^* = 1.00$

<u>t</u> (sec)	<u>T</u> (°R)	<u>P</u> (psia)	<u>T*</u>	<u>P*</u>	<u>M*</u>
0	530	11.3	1.000	1.00	1.00
5	533	22.2	1.016	1.50	1.43
10	545	29.6	1.029	2.00	1.94
15	552	37.0	1.040	2.50	2.40
20	556	44.4	1.050	3.00	2.85
25	561	51.8	1.059	3.50	3.31
30	564	59.2	1.065	4.00	3.79
35	567	67.4	1.070	4.55	4.29
40	570	74.6	1.074	5.05	4.71
45	571	82.2	1.075	5.55	5.17
50	572	89.5	1.080	6.05	5.60
60	575	103.0	1.085	6.95	6.40
70	577	113.6	1.090	7.74	7.10

Table 15
(continued)

Run 17

Orifice: 1/4 in. dia.

$w_0 = 704$ lb/hr

$C_0^* = 10.0$

$T_1^* = 1.00$

<u>t</u> (sec)	<u>T</u> (°R)	<u>P</u> (psia)	<u>T*</u>	<u>P*</u>	<u>M*</u>
0	527	14.8	1.000	1.00	1.00
5	541	26.7	1.026	1.80	1.75
10	550	33.5	1.043	2.60	2.49
15	556	51.1	1.056	3.45	3.27
20	562	63.6	1.065	4.30	4.04
25	566	77.0	1.073	5.20	4.84
30	570	91.0	1.081	6.15	5.68
35	573	103.6	1.088	7.00	6.43
40	577	113.9	1.095	7.70	7.04

Run 18

Orifice: 5/16 in. dia.

$w_0 = 1104$ lb/hr

$C_0^* = 10.0$

$T_1^* = 1.00$

<u>t</u> (sec)	<u>T</u> (°R)	<u>P</u> (psia)	<u>T*</u>	<u>P*</u>	<u>M*</u>
0	531	14.8	1.000	1.00	1.00
2.5	538	24.0	1.017	1.62	1.60
5	547	33.3	1.032	2.25	2.13
7.5	555	42.9	1.045	2.90	2.77
10	560	52.4	1.055	3.54	3.35
12.5	565	62.2	1.064	4.20	3.95
15	568	71.7	1.071	4.85	4.53
17.5	571	81.6	1.076	5.52	5.13
20	574	91.6	1.081	6.20	5.73
22.5	576	102.2	1.086	6.90	6.36
30	578	112.0	1.090	7.56	6.94

Table 16

Blowdown Data - Insulated Tank with
Added Capacitors

Run 19

Orifice: 5/16 in. dia. w_0 - 255 lb/hr C_o^* - 1.44

<u>t</u> (sec)	<u>T</u> (°R)	<u>P</u> (psia)	<u>T*</u>	<u>P*</u>	<u>M*</u>
0	573	111.5	1.000	1.000	1.000
5	567	103.7	.990	.930	.940
10	561	98.0	.980	.880	.898
15	556	91.4	.971	.820	.845
20	552	87.0	.964	.780	.810
25	548	80.8	.955	.725	.760
30	544	73.5	.950	.705	.742
35	542	74.6	.946	.670	.706
40	539	71.0	.940	.637	.677
45	536	67.3	.947	.603	.644
50	534	63.5	.931	.570	.612
55	531	60.2	.926	.540	.583
60	529	55.7	.922	.500	.542
65	526	51.3	.918	.460	.502
70	524	45.8	.914	.412	.450

Run 20

Orifice: 3/8 in. dia. w_0 - 356 lb/hr C_o^* - 1.44

<u>t</u> (sec)	<u>T</u> (°R)	<u>P</u> (psia)	<u>T*</u>	<u>P*</u>	<u>M*</u>
0	577	112.6	1.000	1.000	1.000
5	570	104.5	.989	.930	.940
10	565	96.6	.979	.860	.879
15	558	88.7	.968	.790	.816
20	553	82.0	.959	.730	.762
30	543	70.2	.941	.625	.664
35	538	65.2	.934	.580	.622
40	535	59.6	.927	.530	.572
45	531	52.8	.920	.470	.512
50	527	46.6	.914	.415	.454

Table 16
(continued)

Run 21

Orifice: 7/16 in. dia. $w_0 = 497$ lb/hr

$C_o^* = 1.44$

<u>t</u> (sec)	<u>T</u> (°R)	<u>P</u> (psia)	<u>T*</u>	<u>P*</u>	<u>M*</u>
0	573	111.4	1.000	1.000	1.000
2.5	568	105.4	.993	.945	.952
5	565	100.3	.986	.900	.913
7.5	560	94.5	.973	.850	.868
10	557	90.1	.972	.810	.833
12.5	554	85.5	.966	.768	.795
15	550	81.2	.960	.730	.760
17.5	545	76.6	.952	.688	.730
20	542	72.4	.946	.650	.687
22.5	538	67.9	.940	.610	.650
25	536	63.8	.935	.573	.613
27.5	533	59.6	.930	.536	.577
30	530	55.6	.925	.500	.541
32.5	527	51.2	.920	.460	.500
35	525	47.2	.916	.424	.463

thesM987

An experimental investigation of the eff



3 2768 001 92594 4

DUDLEY KNOX LIBRARY